

# UCLA

## UCLA Previously Published Works

### Title

Reverse osmosis membrane biofouling: causes, consequences and countermeasures

### Permalink

<https://escholarship.org/uc/item/70n5p7mc>

### Journal

npj Clean Water, 5(1)

### ISSN

2059-7037

### Authors

Hoek, Eric MV  
Weigand, Timothy M  
Edalat, Arian

### Publication Date

2022

### DOI

10.1038/s41545-022-00183-0

Peer reviewed

## REVIEW ARTICLE OPEN



# Reverse osmosis membrane biofouling: causes, consequences and countermeasures

Eric M. V. Hoek<sup>1,2</sup>, Timothy M. Weigand<sup>1</sup> and Arian Edalat<sup>3</sup>

Biofouling has been referred to as “the Achilles heel” of reverse osmosis (RO) membrane technology; the main cause being polyamide RO membranes lack of chlorine tolerance. Biofouling increases the operating cost of water treatment by increasing RO system feed pressure (i.e., energy demand) and increasing membrane cleaning frequency, which increases downtime and reduces membrane useful life. For waters with known high biofouling potential, plant designs also may require more extensive pretreatment, which increases capital and operating costs as well as the footprint of a desalination plant. It is known from the literature that the three keys to fending off biofouling in RO systems and/or recovering from biofouling once it takes root include (1) understanding site-specific processes governing biofilm formation, (2) implementing effective biofouling pretreatment ahead of RO membranes, and (3) monitoring biofouling to enable more proactive and effective RO membrane cleaning. Herein, we present four case studies of RO membrane biofouling in seawater, municipal wastewater, brackish groundwater and industrial wastewater. Next, we describe what is known about the causes and consequences of bacterial biofilm formation and growth through a process level RO membrane biofouling model. Finally, we review common biofouling control methods including pre-treatment, chemical cleaning and the most common strategies for monitoring biofouling in RO membrane systems.

*npj Clean Water* (2022)5:45; <https://doi.org/10.1038/s41545-022-00183-0>

## INTRODUCTION

A number of general reviews have been written on various aspects of bacterial adhesion, biofilm formation and biofouling<sup>1–3</sup>. Several reviews specifically focus on biofouling in RO membrane systems<sup>4–9</sup>. Most historical research—both laboratory and field scale—has focused on seawater RO desalination membrane plants with some emphasis on wastewater RO reuse plants. Not much has been reported in the open literature on RO systems processing brackish groundwater or industrial water and wastewater, but we demonstrate herein that biofouling also occurs in these applications.

Biofouling increases trans-membrane (“TMP”) and feed-to-brine trans-module hydraulic pressure losses (“differential pressure” or “delta P”). Biofouling can lead to “biofilm-enhanced concentration polarization” (BCEP), which increases solute passage—degrading product water quality, and also, elevating trans-membrane osmotic pressure, which causes further flux decline. Moreover, biofouling increases the overall cost of water treatment by demanding more pretreatment, increasing RO system operating pressure (i.e., energy demand), increasing membrane cleaning frequency and reducing membrane useful life<sup>10–12</sup>. The keys to fending off biofouling in RO systems or recovering from biofouling once it takes root include

- (1) Understanding site-specific processes governing biofilm formation,
- (2) Implementing effective biofouling pretreatment ahead of RO membranes, and
- (3) Monitoring biofouling to enable more proactive and effective membrane cleaning.

Herein, we describe (1) direct evidence of biofouling occurrence and impacts from four case studies at seawater, brackish

groundwater, municipal wastewater and industrial wastewater RO plants, (2) what is known from the literature and personal experience about the mechanisms and causes of bacterial biofilm formation and growth, (3) what can be deduced from modeling regarding the mechanisms and consequences of RO membrane biofouling at a process level, and (4) the most effective countermeasures for minimizing, mitigating and monitoring biofilm formation in RO membrane systems.

## FOUR CASE STUDIES OF RO MEMBRANE BIOFOULING

### Pacific Ocean water

Autopsy analyses were performed on RO and nanofiltration (NF) membranes extracted from a 1136 m<sup>3</sup> d<sup>-1</sup> (300,000 gallons per day) seawater RO demonstration plant located in Long Beach, California, USA. The plant was split into two trains—one comprised of a single-pass seawater RO configuration and the other a two-pass seawater NF-NF configuration<sup>13</sup>. Pre-treatment ahead of both trains comprised coarse filters, chlorination, 0.1 μm microfiltration (MF), dechlorination (via sodium bisulfite) and 1 μm cartridge filters. Used NF and RO spiral wound elements (SWEs) were removed from the first and last positions of the demonstration plant. The selected membranes represent different stages of operation including (1) new, (2) fouled, and (3) cleaned membranes. Although operating data suggested little outward signs of membrane fouling—inorganic, organic, and bacterial accumulation were identified on all membranes. First pass RO and NF membranes contained similar amounts of deposited solids, while significantly fewer solids were found on second pass NF membranes. Chemical cleaning recovered the performance of both first pass RO and second pass NF membranes, but was relatively ineffective at removing deposited solids from first-pass

<sup>1</sup>University of California, Los Angeles (UCLA); Department of Civil & Environmental Engineering, California NanoSystems Institute, and Institute of the Environment & Sustainability, Los Angeles, CA, USA. <sup>2</sup>Energy Technologies Division, Lawrence Berkeley National Lab, Berkeley, CA, USA. <sup>3</sup>Pacifica Water Solutions, Northridge, CA, USA.

<sup>✉</sup>email: emvhoek@ucla.edu

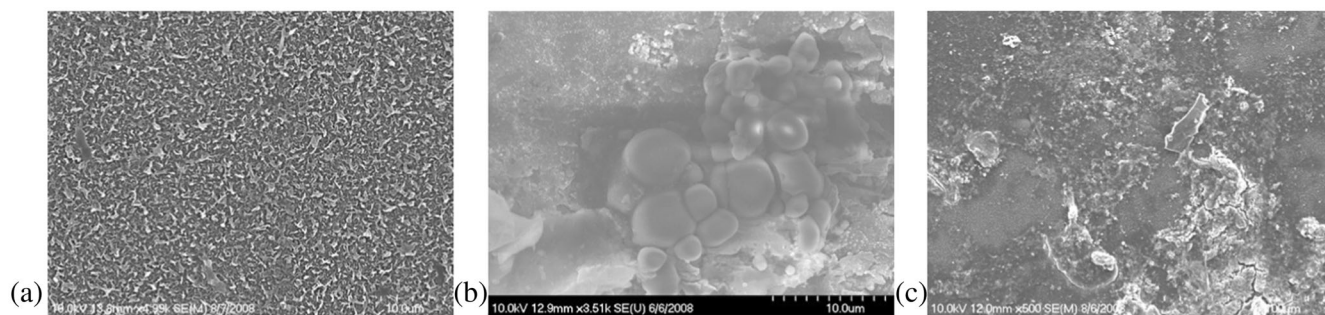


**Fig. 1 Scanning electron microscope images of NF membranes at a seawater desalination plant.** Virgin (a), fouled (b) and cleaned (c) NF membranes from the Long Beach Water Departments's (Long Beach, California, USA) seawater desalination plant<sup>13</sup>. Copyright Desline.

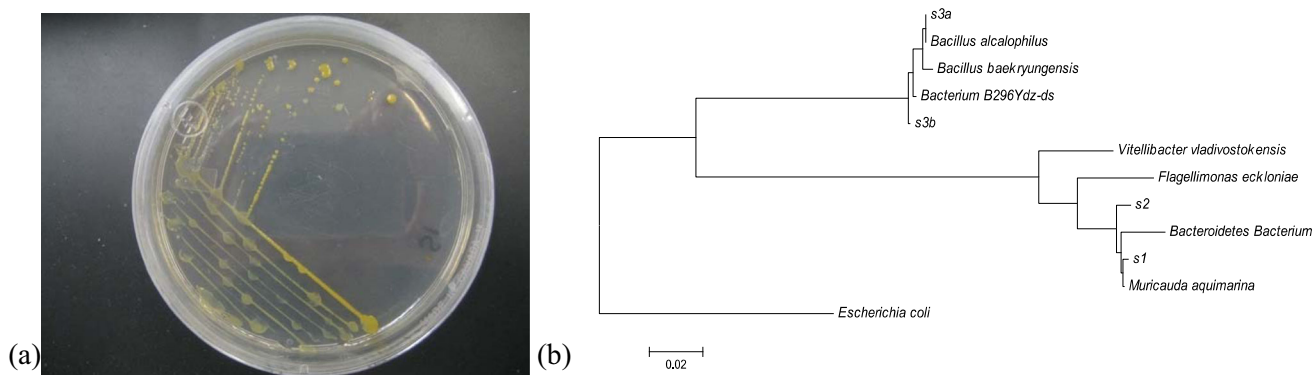


**Fig. 2 Bacteria culture and phylogenetic tree from brackish groundwater RO plant.** Unpublished culture plate image (a) and published phylogenetic tree (b) from the cited RO membrane autopsy project at the Long Beach Water Departments's (Long Beach, California, USA) seawater desalination plant<sup>15</sup>. Copyright Desline.

NF membranes (Fig. 1). Viable, culturable marine bacteria were observed on all fouled and cleaned membranes, indicating that bacterial colonization of seawater NF/RO membranes was not (a) detected by plant performance monitoring devices, (b) prevented by microfiltration and chlorination, or (c) removed by chemical cleaning.

In this same study<sup>13</sup>, molecular analyses revealed a phylogenetic tree of 16S rRNA gene sequences showing an array of both marine and groundwater species (*Bacillus* and *Sporolactobacillus* species) as well as *Escherichia*, *Vitellibacter*, *Flagellimonas*, *Muricauda* and *Flavobacterium* genus. Different pre-treatments were explored and chlorine dioxide was most effective at minimizing biofouling in first pass RO and NF membranes, whereas activated carbon and UV were less effective. In a separate study, the microbial ecology colonizing ten seawater desalination plants from five different global locations (5-California, USA; 1-Florida, USA; 2-Perth, Australia; 1-Gold Coast, Australia, 1-Ashkelon, Israel), was assessed at different stages of treatment processes (intake, cartridge filtration, and SWRO) using both culture-based and molecular methods<sup>14</sup>. At one plant, bacteria colonizing SWRO membranes seemed to represent a sub-population of bacteria present in the influent seawater, and they were quite different from those colonizing the cartridge filter. On SWRO membranes from five different global locations, about 30% of colonized bacteria types were the same regardless of location, whereas influent seawater microbial ecology varied significantly based on location and season.

### Brackish groundwater

Membrane autopsies were performed on low-pressure RO membranes being used in a municipal brackish groundwater RO plant (Arcadia Groundwater Desalter, Santa Monica, California, USA)<sup>15</sup> (Fig. 2). The plant's onsite pre-treatment sequence comprised chlorination, greensand filtration, dechlorination, 5 μm cartridge

filters and antiscalant addition for carbonate scale inhibition. The plant draws groundwater from multiple well-fields and some of the feed waters are filtered through granular activated carbon filters prior to mixing at the RO plant. The RO plant is a 3-stage 4:2:1 array designed to operate at 85% recovery. Membranes from all three stages were autopsied.

The major ailment that affected the plant's performance was a combination of biofouling and silica scaling; the former caused by excessive biogrowth in cartridge filters (CFs)—due to dechlorination occurring ahead of the CFs—and sloughing off of biomass onto the RO membranes, the latter caused by the super-saturated silica content in feed water while operating the RO plant at an unsustainably high recovery (82–85%) given the influent silica concentration (~80 mg/L). A small amount of bacterial colonization was confirmed throughout the plant via Gram staining and light microscopy (Fig. 3, top). Scanning electron microscopy (SEM) and energy-dispersive X-ray (EDX) spectroscopy confirmed biofouling and heavy silica scaling as well as some calcium and magnesium scaling (Fig. 3, bottom). The plant moved the dechlorination unit after the CFs and biofouling was greatly diminished; also, the plant added a silica-selective antiscalant to achieve stable operation at the target recovery.

### Municipal wastewater

Representative images of a biofouled low-pressure RO membrane element from the original Water Factory 21 at the Orange County Water District (OCWD) (Fountain Valley, California, USA) reveal a massive biofilm (Fig. 4a)<sup>16</sup>. The biofilm resembles a dense gel layer to the naked eye, but upon inspection by scanning electron microscopy whole bacteria cells and macromolecular material could be seen. The fouled RO membrane images are from previous operations at OCWD, where feed water passed through conventional secondary wastewater treatment at the neighboring

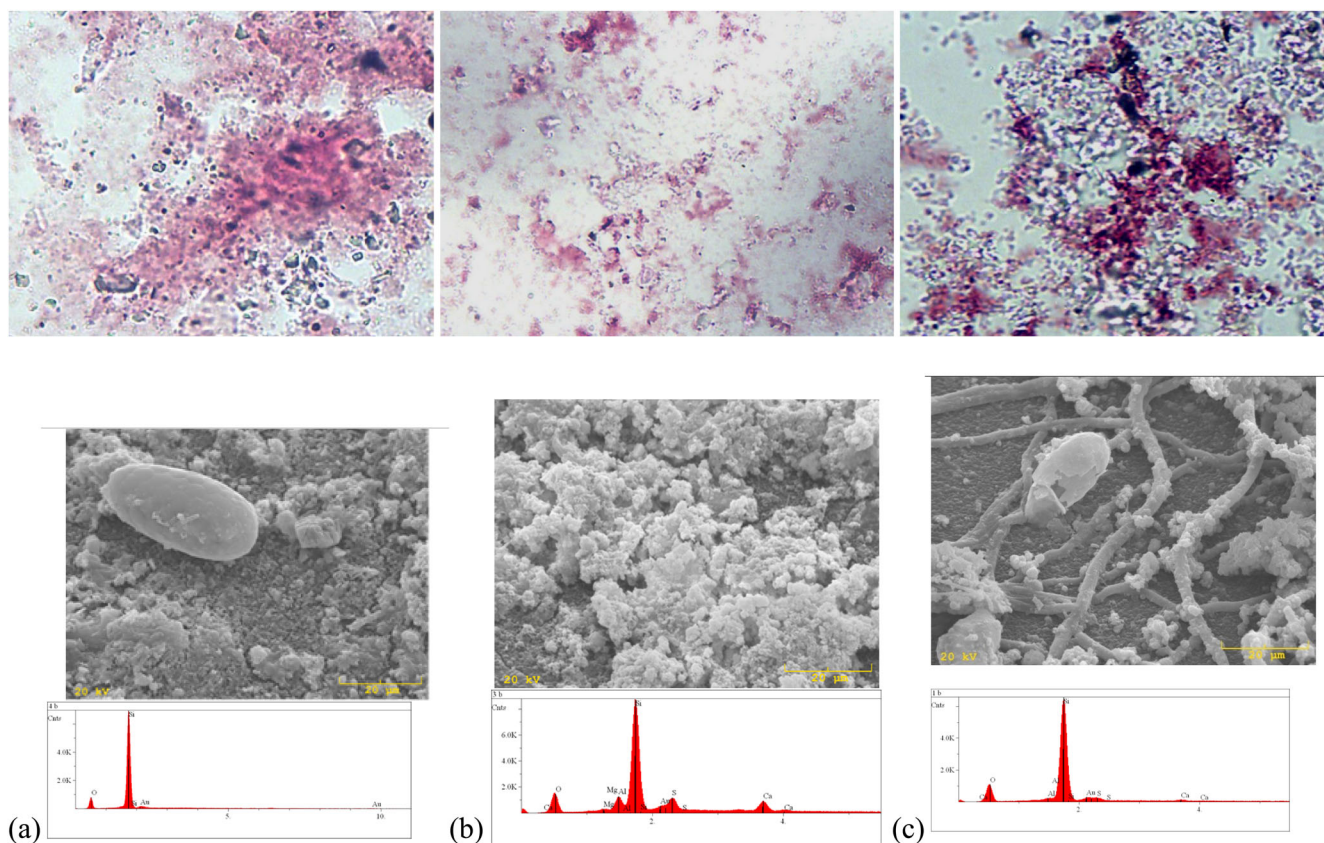


**Fig. 3** Optical and scanning electron microscope images and energy-dispersive analysis of X-rays for membranes at a brackish groundwater RO plant. Previously unpublished light microscopy with Gram staining (top), SEM images (middle) and EDX (bottom) spectra from (a) first stage, lead element, (b) second stage, tail element and (c) third stage, tail element of the City of Santa Monica's Arcadia brackish groundwater desalination plant (Santa Monica, California, USA).

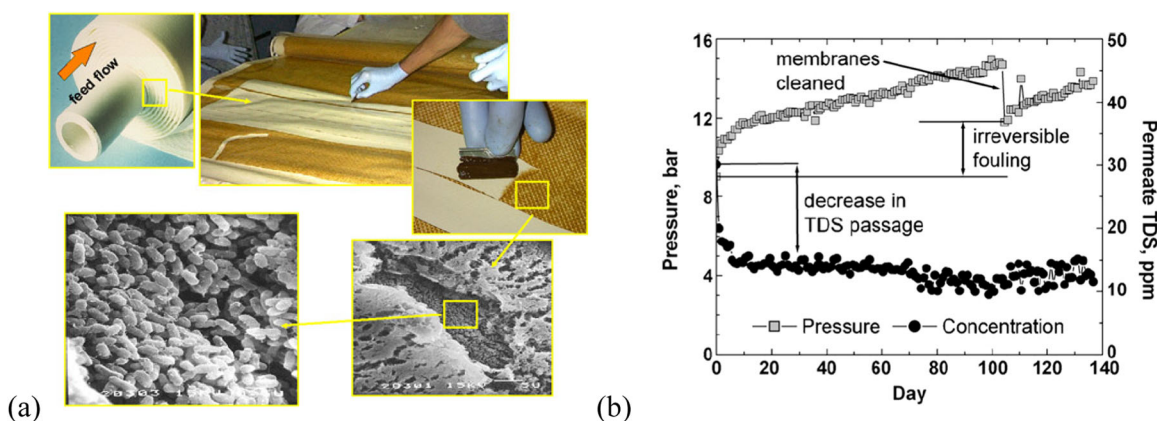


**Fig. 4** Images and data indicating biofouling at a municipal water recycling RO plant. **a** Pictures and SEM images of biofilms formed on RO membranes at the Orange County Water District (Fountain Valley, California, USA).<sup>16</sup> **b** Feed pressure (gray squares) and permeate TDS (black circles) for the duration of the 140 day pilot study. Copyright Elsevier.

Orange County Sanitation District (OCSD); this included screening, primary clarification, biological treatment, and secondary clarification. Additional pretreatment at OCWD included lime-soda softening, polymer flocculation, sedimentation, media filtration, and acidification prior to being fed into the RO membranes depicted. The historic biofouling problem at OCWD derived from microbial re-growth occurring between the pretreatment processes and the RO system due to incomplete disinfection of microorganisms. It has since been corrected through the design and implementation of the 100+ million gallons per day

Groundwater Replenishment System, which employs combined chlorine (chloramines) and MF membranes ahead of the RO membranes without dechlorination. However, some fouling still occurs due to effluent organic matter that passes through MF pretreatment as shown in the pilot system test data (Fig. 4b); the full scale plant is reported to behave similarly<sup>17</sup>.

#### Industrial (steel refinery) wastewater

In a previous study, membrane autopsies were performed after pilot testing of a RO-based water reuse system designed to treat

inorganic wastewater at a steel refinery in South Korea<sup>18,19</sup>. The system employed a 10 µm disk filter and 0.3 µm MF membranes ahead of RO membranes. Fluoride salts of calcium, aluminum, and iron, phosphate salts of calcium and aluminum, as well as organic and bacterial foulants were found on the RO membrane surface (Fig. 5a). In addition, tests for iron-related bacteria (IRB), slime-forming bacteria, sulfate-reducing bacteria (SRB) and heterotrophic aerobic bacteria (HAB) were all positive whereas denitrifying bacteria tests were negative. Gram staining tests of cultures grown on fouling materials extracted from the RO membranes showed predominantly Gram-negative bacteria, which have an outer membrane that makes them more resistant to detergents and biocides. The morphology of the bacteria was mainly spherical cocci, filamentous and rod-shaped organisms. (Fig. 5b). During pilot testing, the RO membrane experienced dramatic increase in feed pressure and loss of salt rejection; the autopsied membranes exhibited signs of mechanical damage, some chemical damage, biological fouling and mineral scaling<sup>18,19</sup>. About half of the mass of fouling materials extracted from the membranes was biofouling related and about half was from inorganic scaling. It was recommended that in the full-plant design some form of chemical softening be implemented as well as chlorination, microfiltration and dechlorination to reduce the influent fouling content and to better protect the RO membranes from subsequent damage.

### Summary and lessons learned

Here, we summarize a few key take-aways from the above four case studies. First, biofouling is a nearly ubiquitous problem for RO membranes, regardless of influent water origin, influent water quality, RO system design and operation as well as physical and chemical pre-treatments. Second, biofouling rarely occurs alone, but rather almost always occurs in conjunction with other forms of fouling and scaling. Thirdly, the appropriate countermeasure for biofouling is site specific and is a function of influent water quality, the RO system design, and environmental conditions. Finally, the only universal attribute that can be identified is the lack of chlorine tolerance by RO membranes, which prevents continuous disinfection and biogrowth controls. Table 1 summarizes the water type, causes, consequences and countermeasures taken in the four case studies presented above.

## CAUSES OF RO MEMBRANE BIOFOULING

### Biofilm formation and growth

Flemming, Ridgway and co-workers conducted pioneering research on RO membrane biofouling 20–30 years ago<sup>5,6,8,20</sup>. Their work elucidated fundamental physical, chemical, and biological factors governing biofouling in real RO membrane plants. Later, Hoek and co-workers studied bacterial deposition, adhesion, and removal from polymeric filtration and desalination membranes<sup>21–27</sup> as well as physical-chemical characteristics and bacterial phylogeny of biofilms formed in several different RO membrane plants<sup>13,14</sup>. Vrouwenvelder and co-workers have focused on bacterial biofilm formation, bio-growth, inhibition, and monitoring in a combination of theoretical, laboratory, and field studies<sup>28–49</sup>. Fane and co-workers also studied RO membrane biofouling causes, consequences, inhibition, and monitoring via several unique methods<sup>50–55</sup>.

In general (Fig. 6), bacteria present in RO feed waters undergo transport to the membrane surface where initial (reversible) adhesion occurs (Stage 1). Irreversible adhesion is associated with biosynthesis of extracellular polymeric substances (EPS) (Stage 2) and a dense biofilm results from bacterial growth and replication at the expense of feedwater nutrients (Stage 3). Complex biofilm formation ensues, which involves communication (quorum sensing) and gradient formation of biological functions among cells

located in different zones of the biofilm (Stage 4). Eventually, a fully formed biofilm sloughs off both viable bacteria cells and nonviable cell debris (e.g., nutrients) to downstream locations; this is known as “dispersal” (Stage 5).

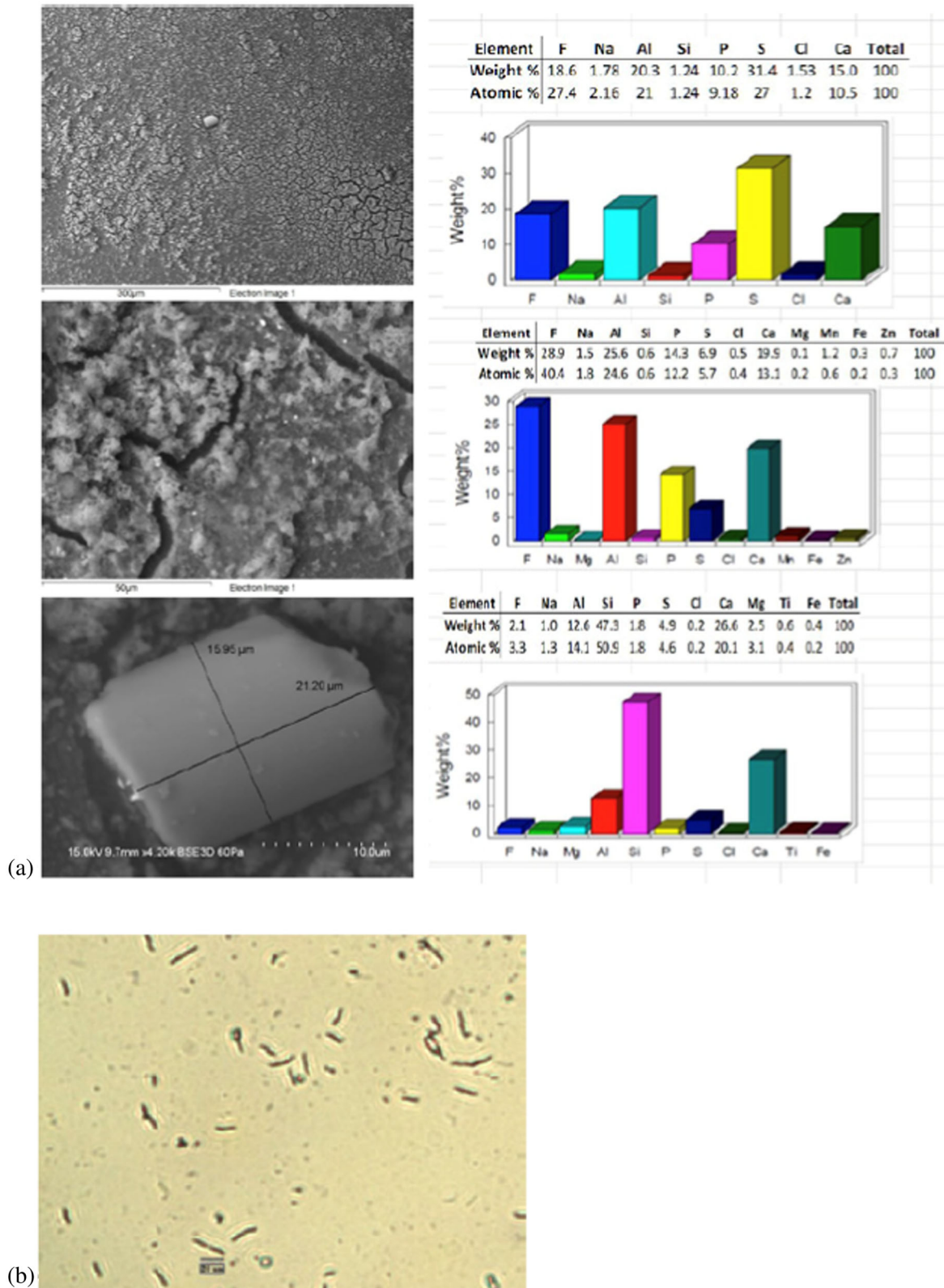
With some exceptions, many academics and practitioners believe bacterial deposition (Stage 1) is of limited consequence in real RO plants, and that, “biofouling is a bio-growth problem.” Proper pre-treatment including chlorination and media or membrane filtration should leave little-to-no viable bacteria cells available to deposit onto RO membranes in a desalination plant. However, improperly designed pre-treatment sequences, which are discussed in more detail in the Section “Sources of nutrients in RO plants that promote bio-growth” below, can deliver nutrients and/or bacteria cells to “seed” biofouling on RO membranes. It should be noted that membrane manufacturing facilities are not sterile environments; hence, RO spiral wound elements may come “seeded” with small amounts of viable bacteria from the point of manufacturing. Possible sources of bacterial contamination include airborne bacteria (bioaerosols) in the building air or from employees coughing or sneezing in the manufacturing space, direct contact from bacteria on employees’ hands, and/or wet-testing of RO membranes using non-sterile tap water or RO permeate.

### Sources of nutrients in RO plants that promote bio-growth

In general, the assimilable organic carbon (AOC) content of the influent natural organic matter (NOM) drives bio-growth throughout a water treatment plant<sup>49</sup>. Bacterial EPS is primarily responsible for hydraulic and osmotic losses from biofilms on RO membranes<sup>10</sup>. Cells starved of AOC do not produce much EPS and so RO membranes may be significantly colonized, but biofouling may not be noticeable until adequate AOC becomes available. During algae blooms, the influent dissolved AOC content at seawater RO plants can be elevated even if algal biomass is removed by pre-filtration; at wastewater recycling RO plants, occasional upsets at the upstream wastewater treatment plant can send more AOC into the downstream RO and induce biofouling events. *Alternatively, brackish groundwater often contains less than 1 ppm of influent total organic carbon (TOC) of which only a fraction comprises AOC, and rarely would TOC fluctuate dramatically such that excursions in AOC concentrations would be sufficient to drive a biofouling event*<sup>56</sup>. So why does it happen?

At RO plants with low influent AOC, pretreatment chemicals can introduce enough AOC into RO membrane systems—over and above the influent NOM-derived AOC—to stimulate significant bio-growth and biofouling<sup>57</sup>. For example, Vrouwenvelder observed metabolically active biofilm bacteria, despite low AOC levels in an RO plant feed water; however, an increase in AOC was observed following the addition of acid (to prevent CaCO<sub>3</sub> scaling) which coincided with a high biofilm formation rate observed through a significant increase in net differential pressure (NDP)<sup>43</sup>. More recently, a well-controlled laboratory study suggests a significant increase in biofilm formation on RO membranes in the presence of both polyacrylate-based (PAA) and polyphosphonate-based (PPP) antiscalants<sup>11</sup>. The PAA increased biofilm formation by membrane surface modification which enhanced bacterial adhesion, while the PPP most likely accelerated biofilm formation by serving as an additional source of phosphorous which is often a limiting nutrient in water treatment systems<sup>35,58</sup>. *Therefore, selection of acid and antiscalant products should take into account their potential contribution to site specific membrane biofouling.*

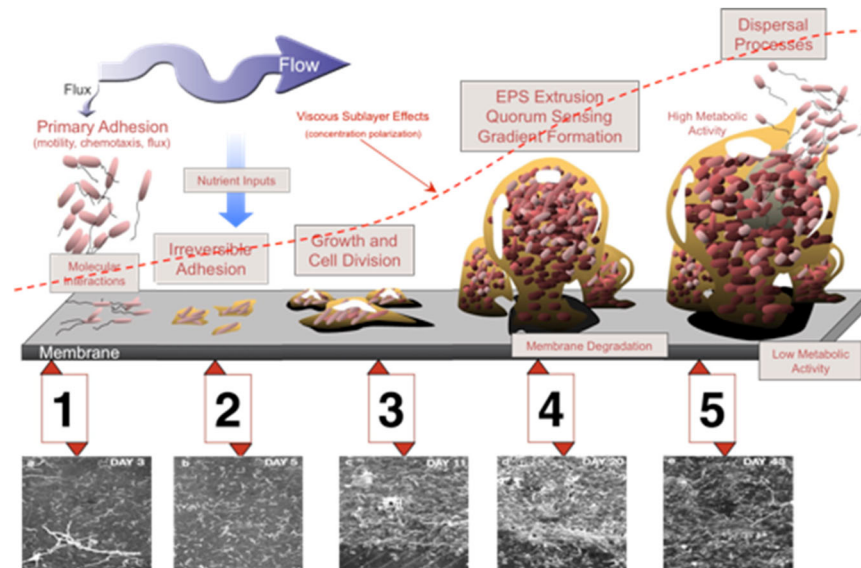
According to Saeed, another important consideration for plants using chlorine for disinfection is the location of sodium metabisulfite (SBS) injection<sup>59</sup>. Typically, SBS is used to remove chlorine ahead of RO membranes to prevent their degradation. Saeed observed reduced RO membrane biofouling potential when the SBS dosing point was placed between dual media filters and



**Fig. 5** Microscopic image of gram-negative bacteria presented on the RO membrane. **a** SEM images of fouled membrane surfaces at different magnifications; scale bars indicate 300, 50 and 10  $\mu\text{m}$  lengths and the crystal is measured at 15.95 x 21.20  $\mu\text{m}$ . **(b)** Relative weight percent by element from different locations of the fouling layer as determined by EDAX. **(c)** Optical microscope image of gram-negative bacteria presented on the RO membrane. The morphology of the bacteria was determined to be mainly spherical cocci, filamentous and rod-shaped organisms.<sup>19</sup> Copyright Industrial Water Treatment.

**Table 1.** Summary of biofouling causes, consequences and countermeasures from case studies.

Water type	Cause(s)	Consequence(s)	Countermeasure(s)
Pacific Ocean water	Naturally occurring and chlorine-derived assimilable organic carbon (AOC)	Subtle flux decline, subtle to no increase in differential pressure	Chemical cleaning to recover clean membrane permeability
Brackish groundwater	Dechlorination ahead of cartridge filter causing biogrowth and sloughing onto RO membranes	Dramatic feed and differential pressure increase and biofilm formation along with silica scaling from lead to final stage	Initial: move dechlorination after cartridge filter and add silica antiscalant Final: switch to continuous chloramination
Municipal wastewater	Insufficient disinfection and residual AOC in tertiary wastewater causing biogrowth	Dramatic increase in feed and differential pressure due to organic and biofouling	Initial: switch from conventional pre-treatment to chlorination, MF and dechlorination Final: switch to continuous chloramination
Industrial wastewater	High hardness, alkalinity particulates and total organic carbon (TOC) in industrial effluent	Dramatic increase in feed and differential pressure due to biofouling and mineral scaling	Initial: add chemical softening to reduce the mineral scaling potential Final: add chlorination ahead of MF and dechlorination between MF and RO

**Fig. 6 The five stages of biofouling.** Illustration and SEM images of the five major stages of biofilm formation and growth over time (figure provided by Harry Ridgway<sup>114</sup>).

cartridge filters, but higher biofouling potential was observed as the SBS dosing point was moved forward along the pretreatment line, closer to the RO membranes. It is known that antiscalants can be oxidized by traditional water disinfectants and oxidants. Therefore, even when using antiscalant and acid products with quantifiably low AOC, one must consider the possibility that locating the antiscalant and/or acid injection point prior to SBS injection could lead to oxidation and enhanced biodegradability of either (1) antiscalant polymers or (2) the non-oxidative biocides used in acid and antiscalant formulations. This could introduce AOC formation just as the water enters the RO membrane system and over-time lead to a biofouling problem. Accordingly, the location of SBS dechlorination relative to acid and/or antiscalant injection points must be considered.

## MODELING RO MEMBRANE BIOFOULING

### Model formulation

Whereas the basic biological aspects of biofilm formation and growth are similar in membrane systems as in natural and

engineered systems, membranes are perhaps uniquely impacted by pressure-driven water and solute transport phenomena that influence biofouling kinetics<sup>8</sup>. Convective delivery of nutrients into and through biofilms enhances nutrient availability, while nutrient concentration polarization (CP) and BECP elevate the concentration of nutrients over the bulk, influent concentration. The growing biofilm constricts feed-to-concentrate flow, thereby enhancing cross-flow velocity, mass transfer, and differential pressure losses.

Somewhere between the biofilm formation Stages 2 and 5 (Fig. 6), symptoms of membrane fouling emerge which could include (i) an increase in resistance to water permeation due to the establishment of a gel-like deposit (i.e., the biofilm), (ii) BECP induced lower solute rejection and increased trans-membrane osmotic pressure ( $\Delta\pi_m$ ), (iii) an increase in the net differential pressure ( $\Delta p_x$ ) across the RO modules, (iv) biodegradation and/or biodeterioration of the membrane polymer or other module construction materials (e.g., polyurethane-based glue lines), and (v) establishment of concentrated populations of primary or secondary human pathogens on membrane surfaces. Here, we model items (i) and (iii) assuming items (ii), (iv) and (v)

are negligible or negligible over the time scale being modeled. These simulations are not meant to be definitive, but merely illustrative exemplars of biofouling dynamics over time through-out an RO system.

In our model, we simulate the pressure, velocity, and the concentration of two solutes, namely, the total dissolved solids (TDS) and a bacteria substrate, in the feed channel of an RO membrane. Transport of water and solutes through the membrane is included in the model as a mass flux out of the system and concentration polarization at the membrane interface is also simulated. Finally, we include a biofouling model that acts to reduce the height of the feed channel as a biofilm grows, increases the resistance to water permeation, and reduces the substrate concentration at the membrane interface through uptake. We assume that the growth of the biofilm layer is sufficiently slow such that the pressure, velocity, and solute concentrations along the length of the feed channel are independent of time.

**Model geometry.** The RO spiral wound elements are assumed to act like a thin rectangular channel containing a typical woven mesh feed spacer in the cross-flow direction. The spacer-filled cross-flow channel is sandwiched between two membranes with the active layers both facing the spacer from top or bottom<sup>16</sup>. The curvature of the spiral wound elements is assumed negligible at the system scale being examined<sup>60</sup>. Complete mixing in the direction orthogonal to the flow was assumed, so that differences in pressure, flow and solute concentration are only computed in the axial (cross-flow) direction, which results in a one-dimensional model. Note that while we assume complete mixing in the feed channel, we consider the effects of concentration polarization at the membrane interface.

**RO system feed channel.** The available hydraulic pressure ( $\Delta p_h$ ) in the feed channel is determined from the cross-flow velocity ( $u$ ) according to

$$\frac{d(\Delta p_h)}{dx} = \frac{-0.5\rho u^2 f_{sp}}{d_h} \quad (1)$$

where  $d_H (=2\epsilon H)$  is the hydraulic diameter,  $H$  is the cross-flow channel height,  $\epsilon$  is the spacer porosity,  $\rho$  is solution density, and  $f_{sp} (=6.23 \cdot \text{Re}^{-0.3})$  is an empirical friction factor that accounts for pressure drop in a mesh spacer-filled cross-flow channel, and  $\text{Re}$  is the cross-flow Reynolds number<sup>61</sup>. The channel height and hydraulic diameter can vary as biofilm grows and we assume axial flow through the biofilm is negligible.

The cross-flow velocity ( $u$ ) is determined from conservation of mass where the height of the channel is varying due to the growth of the biofilm

$$\epsilon \frac{d(uH)}{dx} = -2J_w \quad (2)$$

where  $J_w$  is the water flux through the membrane and occurs through the top and bottom of the feed channel.

A solute concentration ( $c_s$ ) is determined from a species mass balance where the solute may exit only via permeation through the RO membrane. The concentration along the cross-flow channel is given by

$$\epsilon \frac{d(uHc_s)}{dx} = -2J_w c_p \quad (3)$$

where  $c_p$  is the solute permeate concentration. The mass balance of Eq. (3) is the same for the biofilm substrate except that uptake by the bacteria at the membrane interface is also included.

**Transport through the membrane.** The volumetric water flux ( $J_w$ ) through the RO membrane is determined according to the solution diffusion model,

$$J_w = A \cdot (\Delta p_h - \Delta \pi_m) \quad (4)$$

where  $A$  is the intrinsic water permeance (=permeability/thickness),  $\Delta p_h$  is the available hydraulic pressure,  $\Delta \pi_m$  is the trans-membrane osmotic pressure, and the difference between the two is the trans-membrane pressure,  $\Delta p_m = (\Delta p_h - \Delta \pi_m)$ . The trans-membrane osmotic pressure is related to the concentration difference ( $\Delta c_m$ ) across the membrane, which is determined from the intrinsic solute rejection ( $r_s$ ), the salt concentration at the membrane surface ( $c_m$ ) and the osmotic coefficient ( $f_{os}$ ) according to

$$\Delta \pi_m = f_{os} r_s c_m \quad (5)$$

As with the water flux, the solute flux through the membrane ( $J_s$ ) is modeled with the solution diffusion model,

$$J_s = B \cdot \Delta c_m \quad (6)$$

where  $B$  is the intrinsic solute permeance  $\Delta c_m (=c_m - c_p = r_s c_m)$ , and  $c_p$  is the permeate concentration. Solute rejection is a function of the flux and solute permeance, and is defined by

$$r_s = 1 - c_p/c_m = J_w/(J_w + B) \quad (7)$$

The above equations are coupled with pressure, flow, and concentration equations in the feed channel to track all of RO system key performance indicators. Also, the effective  $A$  and  $B$  values are assumed constant, which may not be true in practice due to membrane compaction and/or variations in membrane-active layer<sup>16,62</sup>.

**Concentration polarization.** One of the most important interfacial transport phenomena in RO membrane processes is concentration polarization (CP), which describes the elevated concentration of rejected solutes at the surface of the membrane ( $c_m$ ) to the local feed channel concentration ( $c_x$ ). Here, the CP modulus is determined from

$$CP = c_m \cdot c_x^{-1} = [1 - r_s + r_s \cdot \exp(-J_w \cdot k_s^{-1})]^{-1} \quad (8)$$

where relates the rejection ( $r_s$ ), to the water flux and the solute mass transfer coefficient ( $k_s$ ). The empirical relationship for the mass transfer coefficient for a spacer-filled channel can be estimated from

$$k_s = Sh \cdot D \cdot d_H^{-1} = 0.065 \cdot \text{Re}^{0.875} \cdot \text{Sc}^{0.25} \cdot D \cdot d_H^{-1} \quad (9)$$

where  $\text{Sc}$  is the Schmidt number and  $D$  is the solute diffusivity<sup>61</sup>.

**Biofouling.** The growth of biofilm on the membrane surface increases the resistance to water permeation by adding the additional pressure drop across the biofilm; hence, the available trans-membrane pressure to drive water permeation becomes

$$\Delta p_m = \Delta p_x - \Delta \pi_m - \Delta p_f \quad (10)$$

which replaces the pressure drop in equation (4) when biofouling occurs. Here  $\Delta p_x$  is the available hydraulic pressure,  $\Delta p_f [=J_w \cdot (r_f \delta_f)^{-1}]$  is the pressure drop across the biofilm deposit on top of the membrane,  $r_f$  is the intrinsic hydraulic resistance per unit thickness of biofilm (assumed a constant, which is a source of uncertainty), and  $\delta_f$  is the local biofilm thickness. The biofilm thickness will be determined from a coupled biogrowth model (see the Section "Substrate-limited biofilm growth" below).

Besides increasing the hydraulic pressure drop across the membrane, the biofilm also reduces the effective channel cross-section (i.e., effective hydraulic diameter) as it coats the membrane surface and fills the voids between the spacer filaments. It is assumed that biofilm growth is the same on both membrane surfaces (top and bottom) within the spacer-filled channel, and hence, the channel height is

$$H = H_0 - 2 \cdot \delta_f \quad (11)$$

where  $H_0$  is unfouled channel height. Herein, both membrane degradation (by biofilm microorganisms) and BECP are neglected.



**Substrate-limited biofilm growth.** To model the growth of biofilm on the membrane surface, it was assumed that an initial number of bacteria ( $N_0$ ) were already attached to the membrane. Growth of bacteria was modeled using a substrate-limited growth model assuming bacteria are in an exponential growth phase according to

$$N(t) = N_0 \exp(k_b \cdot c_m \cdot t) \quad (12)$$

Here the number of bacteria per unit area of membrane is a function of the substrate (nutrient) concentration at the membrane ( $c_m$ ), the initial number of bacteria, and the growth rate constant ( $k_b$ )<sup>63</sup>. To relate the number of bacteria to the biofilm thickness, it is assumed that spherical bacteria first grow in a monolayer, in a close-packing arrangement, and once that layer is saturated with bacteria ( $N_{sat}$ ), the thickness of the biofilm ( $\delta_f$ ) increases by the thickness of the bacteria ( $\delta_b$ ). This process continues layer by layer according to

$$\delta_f = \delta_b \cdot N \cdot N_{sat}^{-1} \quad (13)$$

Here loss of biofilm due to sloughing is neglected and deposition of new bacteria is considered negligible. The uptake of the substrate by the biofilm ( $r_{cm}$ ) was modeled by the Eckenfelder relation<sup>63</sup>,

$$r_{cm} = \begin{cases} -Y_s c_m N & \text{if } N \leq N_{max} \\ -Y_s c_m N_{max} & \text{if } N > N_{max} \end{cases} \quad (14)$$

Equation (14) relates the reduction in substrate concentration to the number of bacteria ( $N$  or  $N_{max}$ ), the substrate concentration at the membrane surface ( $c_m$ ) and a substrate utilization rate constant ( $Y_s$ ). As part of the Eckenfelder relation, it is assumed that once the number of bacteria reach a given value ( $N_{max}$ ), only that many bacteria are actively participating in the uptake of the substrate.

**System level key performance indicators.** The five key system level performance indicators include permeate water quality in terms of solute concentration ( $\bar{c}_p$ ), permeate water recovery ( $Y$ ), feed pressure, differential pressure and specific energy consumption (SEC). The system average permeate water quality is determined from

$$\bar{c}_p = \frac{\int_0^L c_p w J_w dx}{\int_0^L w J_w dx}, \quad (15)$$

where  $w$  is the cross-flow channel width. The permeate water recovery is defined as

$$Y = \frac{\int_0^L w J_w dx}{Q_0}, \quad (16)$$

where  $Q_0$  is the volumetric flow rate at the inlet. The specific energy consumptions is

$$SEC = \frac{\Delta p_0}{\eta Y} \quad (17)$$

where  $\Delta p_0$  is the initial applied pressure and  $\eta$  is the pump and motor efficiency<sup>64</sup>.

## Model Implementation

**Approximation methods.** The finite volume approach with one-point upstream weighting was used to solve governing equations for the available hydraulic pressure, velocity, and TDS and substrate concentrations in the feed-channel. The same computational mesh used for the feed-channel solution variables was also used for the transport through the membrane, concentration polarization, and the biofouling model. We assume that the feed-channel and membrane transport models instantly reach a steady-state, thus decoupling these models from the biofilm growth model. The model was run at a constant water recovery value of

85%. To enforce this behavior, the feed pressure was optimized with Newton's Method to allow for this recovery.

**Model parameters.** For illustrative purposes, we considered a full-scale RO system treating low salinity water with sufficient nutrients to promote biogrowth—exemplary of a municipal water recycling scenario. The RO system modeled comprises 3-stages in a "3:2:1" array configuration with seven elements in each stage of pressure vessels. Each SWE is modeled as 1 m long and 0.7122 m wide with 26 leaves. Other system details like membrane permeance, feed water quality, etc. are taken from a previous modeling and pilot plant study<sup>16</sup>, and presented in Table 2. The efficiency of the pumps was assumed to be 80%.

As with the membrane transport parameters, all biofilm parameters except thickness were assumed constant with respect to time (Table 3). Assuming maximum random packing ( $\epsilon = 0.36$ ) of  $1 \mu\text{m}$  diameter spherical bacteria cells, the maximum number of bacteria that could fit in a monolayer on a membrane surface is  $1.143 \text{ cells } \mu\text{m}^{-2}$  ( $1.222 \text{ cells } \mu\text{m}^{-3}$ ); however, the structure of most biofilms is not like a packed bed of spheres. Rather, biofilms are typically comprised of cells, EPS, and water, where (formed in other non-membrane systems) bacterial cell density ranges from about 0.08 to 0.22  $\text{cells } \mu\text{m}^{-3}$  with porosities of 30–80%<sup>65</sup>. From RO membrane autopsies and other studies, bacterial cell density in biofilms are clearly much higher due to compaction from high applied pressure, so here we use a value of  $1.0 \text{ cells } \mu\text{m}^{-2}$ , which gives a porosity of ~47%, and the specific biofilm resistance was assumed to be  $8.4 \times 10^{18} \text{ m}^{-2}$ , which is consistent the biofouling layer that formed in a previous study<sup>16</sup>.

**Table 2.** Values of parameters used in the model.

Parameter	Symbol	Value	Units
Feed flow rate	$Q_f$	180	gpm
Feed pressure	$\Delta p_f$	145	psi
Permeate water recovery	$Y_w$	85	%
TDS concentration	$c_f$	912	$\text{mg l}^{-1}$
Initial channel height	$H_0$	$8.13 \times 10^{-4}$	m
Spacer porosity	$e$	80	%
Osmotic pressure coefficient	$f_{os}$	64,318	$\text{Pa m}^3 \text{ kg}^{-1}$
Friction factor	$f_{sp}$	6.23	-
Membrane water permeance	$A$	$9.33 \times 10^{-12}$	$\text{m}(\text{Pa s})^{-1}$
Membrane salt permeance	$B$	$5.5 \times 10^{-8}$	$\text{m s}^{-1}$
Solute diffusivity	$D_s$	$1.7 \times 10^{-9}$	$\text{m}^2 \text{ s}^{-1}$
Viscosity	$m$	$8.93 \times 10^{-4}$	$\text{Pa s}$
Density	$r$	998.4	$\text{kg m}^{-3}$

**Table 3.** Parameters used for the biofilm portion of the model.

Parameter	Symbol	Value	Units
Maximum bacteria in monolayer	$N_{sat}$	1.0	$\text{cells } \mu\text{m}^{-2}$
Biofilm resistance	$r_f$	$8.4 \times 10^{18}$	$\text{m}^{-2}$
Bacteria growth rate constant <sup>63</sup>	$k_b$	0.044	$\text{L}(\text{mg d})^{-1}$
Inlet substrate concentration	$c_s$	10	$\text{mg L}^{-1}$
New bacteria cell yield	$Y_s$	$8.5 \times 10^{13}$	$\text{cells mg}(c_s)^{-1}$
Maximum bacteria for substrate	$N_{max}$	100	$\text{cells } \mu\text{m}^{-2}$

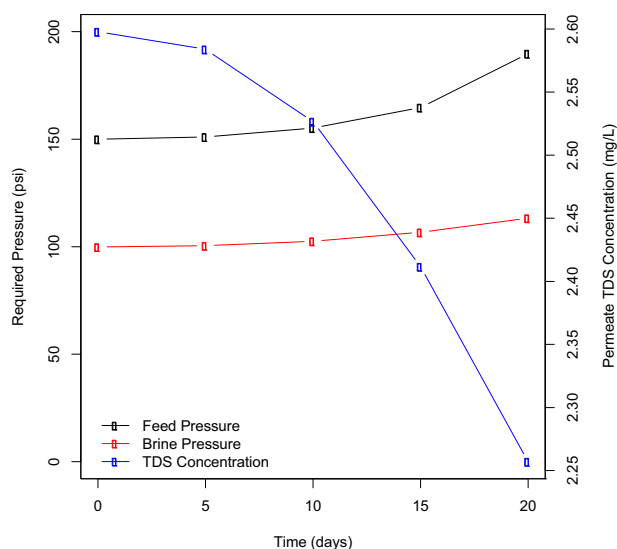


**Fig. 7 Model illustration of biofouling effects on RO membrane system key performance indicators.** Impacts of biofouling on feed pressure, brine pressure and permeate TDS concentration.

**Table 4.** Impact of biofouling on system average key performance indicators.

Day	Feed press. (bar)	Brine press. (bar)	Rejection (%)	SEC (kW-h/m <sup>3</sup> )
0	10.3	6.9	99.72	0.400
5	10.4	6.9	99.72	0.402
10	10.7	7.1	99.73	0.413
15	11.4	7.4	99.74	0.438
20	13.1	7.8	99.76	0.505

## CONSEQUENCES OF RO MEMBRANE BIOFOULING

### System level performance

The feed pressure increases non-linearly over time ultimately increasing ~27% in 20 days (Fig. 7), while the brine pressure increases ~13%, and hence, also contributes to the required feed pressure increase. Permeate TDS remains stable (decreasing slightly) during this 20-day period of biofouling, and so, the system level rejection was also fairly stable ~99.72–99.76%. Operating at constant recovery means that the SEC scales directly with the feed pressure, and hence, increased ~27% (0.4–0.5 kWh/m<sup>3</sup>). We note a lag-time of about 10 days, where biofilm bacteria (in the model) are consuming nutrients and growing a thicker biofilm, but the feed and differential pressure increases are fairly negligible (Table 4). This is a key stage of biofouling, but to understand it better we need to visualize nutrient substrate concentration and biofilm thickness changes over time and throughout the length of the system.

### Local substrate, biofilm, pressure, and flux profiles over time

The biofilm grows at a fairly steady rate over time, but grew most quickly near the entrance of the RO membrane system, by day 20 reaching a thickness of ~200  $\mu\text{m}$  at the inlet and only ~1  $\mu\text{m}$  at the outlet (Fig. 8a). The high growth rate at the inlet of the system is attributed to the substrate (nutrient) concentration being the highest and declining from inlet to outlet as it is consumed by biofilm bacteria. The 200  $\mu\text{m}$  biofilm thickness corresponds to a bacteria surface density of ~10<sup>6</sup> cells/mm<sup>2</sup>, which is consistent with autopsies from biofouled SWEs<sup>66</sup>. It is not clear whether a biofilm would approach 200  $\mu\text{m}$  in a real RO system due to shear forces and sloughing, which may limit the thickness of the biofilm.

Moreover, the biofilm is likely to be highly non-uniform in a given location along the length of the RO system based on the potential existence of flux hot spots and stagnant zones (see the Section “Local substrate, biofilm, pressure and flux profiles over time”). The substrate profiles took a similar shape as the biofilm thickness profiles (Fig. 8b). At day 0, the substrate decreased linearly as the bacterial density is constant throughout the system. As the bacteria density increased more quickly at the inlet, the profile takes a more non-linear shape. The initial slope on days 15 and 20 were equal due to the bacterial density being greater than the maximum bacterial density for substrate uptake ( $N_{\text{max}}$ ). The biofilm was sufficiently active towards the inlet that the substrate was ~80% consumed by the end of the first stage.

As seen from the pressure profiles (Fig. 9), the formation of the biofilm resulted in a large increase in resistance to permeation near the system inlet, and hence, the flux declines in the lead elements and it shifts downstream increasing in the later elements (Fig. 10a). The maximum water flux on day 0 was 9  $\mu\text{m/s}$  and it occurred at the beginning of the first element, whereas on day 20 it was 7.3  $\mu\text{m/s}$  and it occurred at the beginning of the fourth element. Plotting the normalized flux (Fig. 10b) highlights the downstream shift in flux. So, over the course of biofilm growth, the maximum flux comes down and shifts downstream where biofilm thickness drops off; however, to maintain the constant recovery target of 85% more water must permeate through downstream SWEs.

### Additional complications in RO membrane systems

One of the advantages of state-of-the-art polyamide composite RO membranes is their high water permeability, which is achieved (commercially) by tailoring interfacial polymerization chemistry, coating conditions and support membrane skin layer porosity to minimize film thickness, maximize cross-linking density and surface area (roughness) all to minimize the effective path length for diffusion through the composite structure<sup>67</sup>. An unintended consequence of composite RO membranes with rough surfaces is enhanced fouling rates by: (1) enhanced local fouling rates due to flux “hot spots”<sup>68–70</sup> and (2) disproportionately reduced repulsive (e.g., electrostatic and hydrophilic/hydrophobic) interfacial forces<sup>25,71–73</sup>. Localized flux hot spots due to support membrane pores and coating film surface roughness may elevate local fluxes 3–6X higher than the area average flux, which translates into dramatically higher local CP modulus, and hence, higher rates of fouling and scaling. Reduced repulsive interaction forces make rough membrane surfaces appear “stickier”—i.e., more fouling prone and difficult to clean<sup>25,74</sup>.

Another complication, specific to RO membranes, is the presence of mesh feed spacers in the cross-flow channels. Such materials are currently necessary to provide the flow channel and promote mixing via the undulating flow field that develops. While we have empirical models to describe channel-averaged impacts of mesh feed spacers on mass transfer and pressure drop, the role of these feed spacers on CP modulus and biofouling is just beginning to emerge<sup>26,34</sup>. From computational fluid dynamics (CFD) simulations, it appears that wherever the woven mesh spacer contacts an RO membrane surface a stagnant zone forms, in which, localized CP modulus levels for dissolved solutes can spike as high as 1.8–2.0 for certain spacer geometries<sup>75</sup>. For woven mesh spacers, contact occurs predominantly at the “node” where filaments pass over and under each other, whereas for biplanar spacers contact may occur continuously along each filament.

Whereas, it is generally believed that the CP modulus in commercial SWEs is under ~1.1X<sup>16,64</sup>, taking into account the potential impacts of RO membrane surface roughness creating localized flux hot spots and mesh feed spacers creating periodic stagnant mass transfer zones, one can envision elevated localized CP modulus of 2–3X in and around spacers (Table 5).

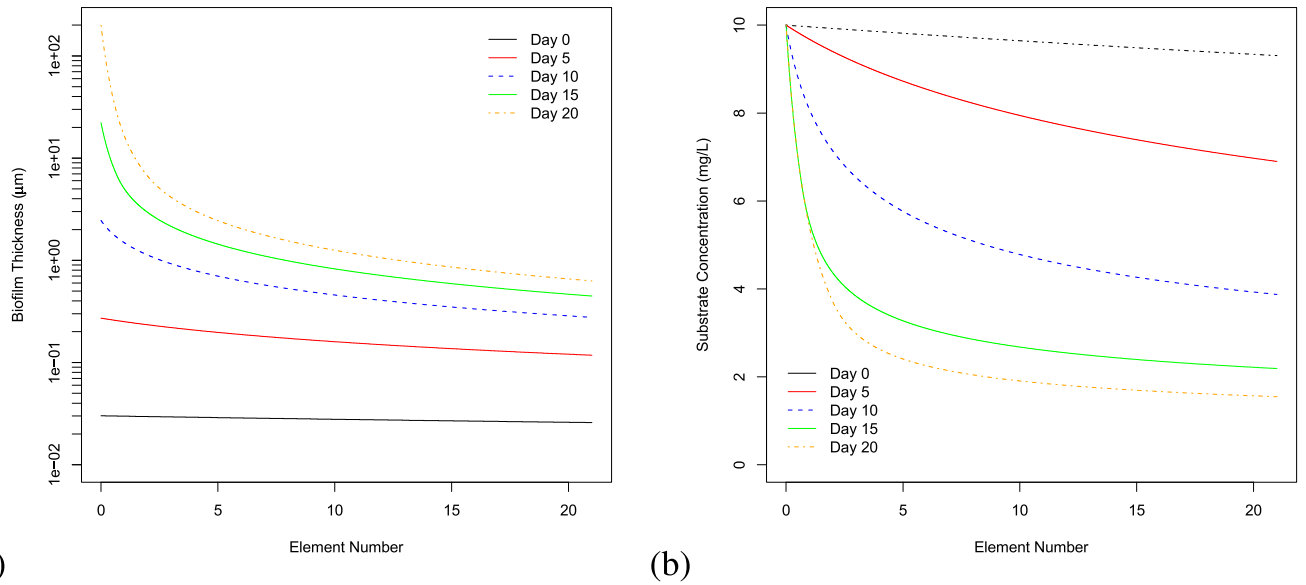


**Fig. 8 Model illustration of local substrate limited biofilm growth kinetics.** Biofilm thickness (a) and substrate concentration (b) profiles from inlet to outlet of the RO system showing that with substrate limited growth kinetics the biofilm grows thickest at the inlet where the substrate concentration is highest with less growth downstream as substrate concentrations drop due to upstream consumption.

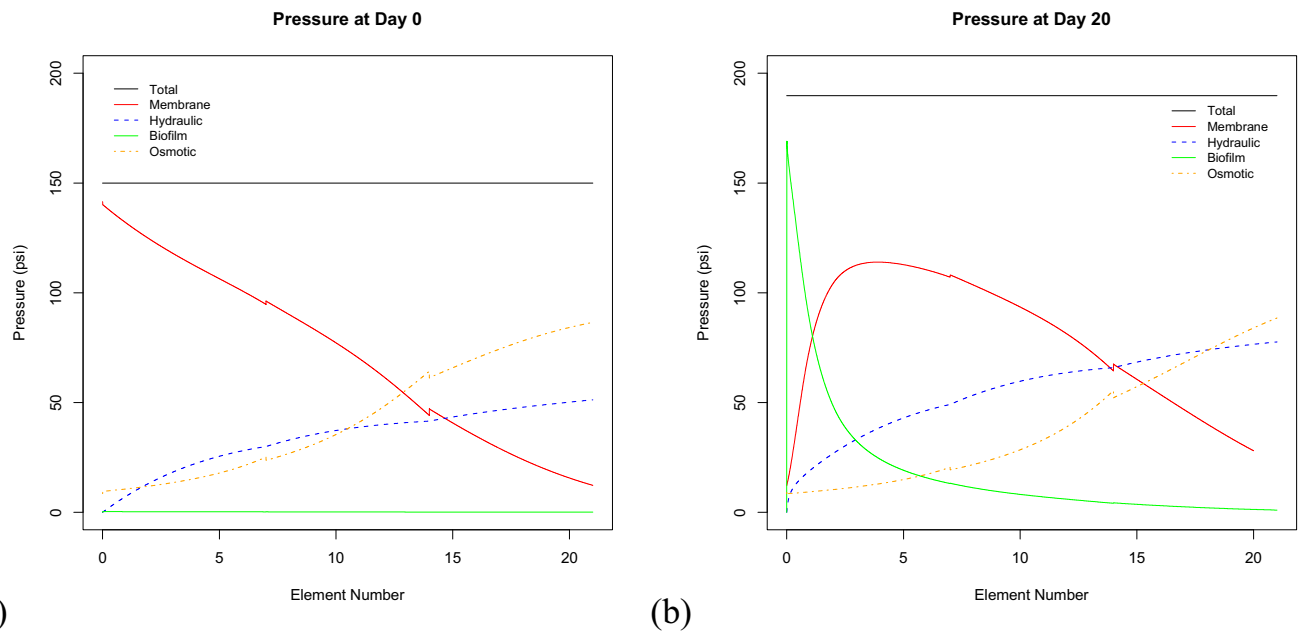


**Fig. 9 Model illustration of local pressure profiles before and after biofilm formation.** Local pressure drops on day 0 (a) and day 20 (b) from inlet to outlet of the RO system illustrating the drop in trans-membrane pressure (TMP) at the inlet where the biofilm initially forms and the shift in TMP downstream as the biofilm pressure drop grows from the plant inlet downstream over time.

Moreover, bacteria cells and nutrients might concentrate in those regions and likely promote faster biofilm formation and growth, at least initially. There is building evidence that the best spacer might be “no spacer” since these mesh feed spacers promote biofouling (and scaling) because of the localized stagnant zones<sup>29</sup>, and they appear to have little positive impact on permeate water quality or energy demand<sup>64</sup>.

#### COUNTERMEASURES OF RO MEMBRANE BIOFOULING

Flemming states<sup>5,6</sup>, “Countermeasures (of RO membrane biofouling) require a three-step protocol: (1) detection, (2) sanitation, and (3) prevention.” Some levels of pre-filtration can reduce the load of

colloidal and particulate matter that directly foul RO membranes through cake formation and cake-enhanced concentration polarization<sup>76</sup>, and also to reduce the influent load of viable biofilm-forming microorganisms<sup>77</sup>. An effective chemical disinfection regime that inhibits bio-growth throughout the RO system greatly improves performance, reliability and economics by reducing the feed pressure, cleaning frequency, cleaning chemical costs, plant downtime and operator intervention<sup>78</sup>.

In addition to pretreatment, each RO membrane plant must develop an optimized approach to RO membrane cleaning (both frequency and chemical regime) as well as RO element rotation and replacement<sup>78</sup>. *However obvious these statements may appear, there is no universally successful combination of pretreatment and*

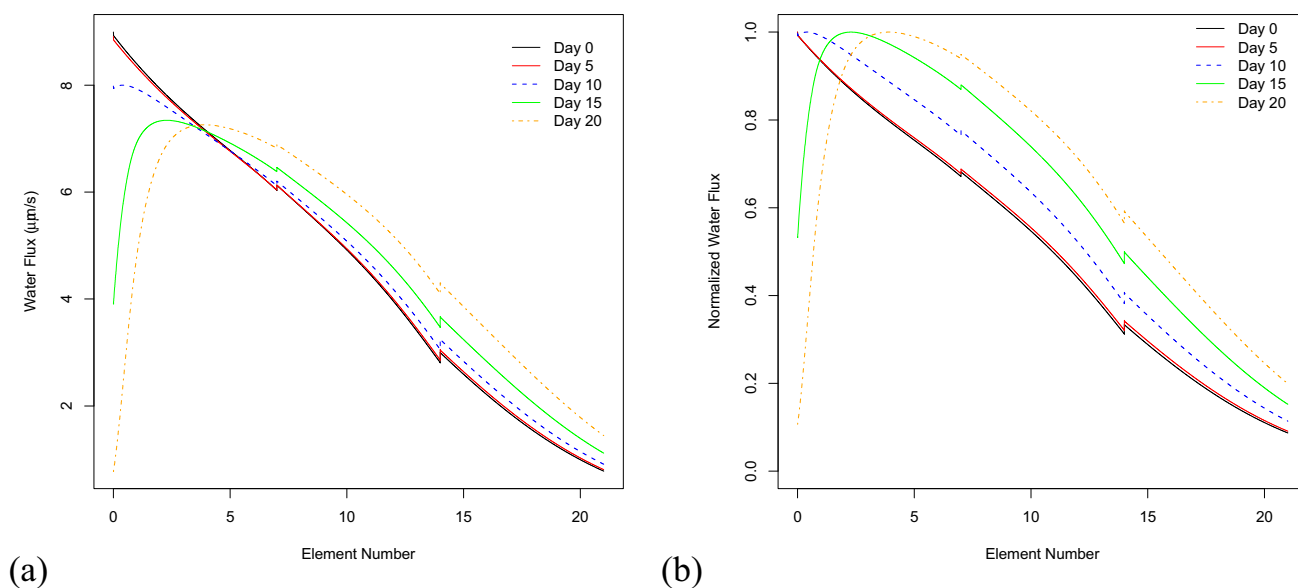


**Fig. 10** Model illustration of local flux profiles before and after biofilm growth. Absolute (a) and normalized (b) permeate flux profiles from inlet to outlet of the RO system illustrating the drop in flux at the inlet where the biofilm initially forms and the shift in flux downstream as the biofilm grows from the plant inlet downstream over time.

**Table 5.** Possible impacts of flux hot spots and stagnant zones.

Item	$J_w$ , m/s	$J_w$ -factor	$k_s$ , m/s	$k_s$ -factor	CP modulus	Basis
1	5.00E-06	1.00	7.00E-05	1.00	1.07	Average flux
2	1.50E-05	3.00	7.00E-05	1.00	1.24	Min hot spot flux
3	3.00E-05	6.00	7.00E-05	1.00	1.54	Max hot spot flux
4	5.00E-06	1.00	7.21E-06	0.10	2.00	Leading stagnation zone
5	5.00E-06	1.00	8.51E-06	0.12	1.80	Trailing stagnation zone
6	These cells intentionally left blank.				3.07	Item 3 × 4 (max × max)
7					2.23	Item 2 × 5 (min × min)

Assumes perfect rejection, so  $CP = \exp(J_w/k_s)$ .

*maintenance. Why? The principal reason is that modern polyamide composite RO membranes cannot be continuously exposed to free chlorine without rapid degradation and loss of rejection. Without the ability to continuously chlorinate a water treatment system, biofouling control becomes complex and subject to a milieu of site-specific nuances.*

#### Use of chemical disinfection to suppress bio-growth

Oxidizing biocides such as chlorine, chloramines, ozone, and chlorine dioxide are commonly used to inhibit bio-growth in water treatment systems and other non-oxidizing biocides and ultraviolet (UV) disinfection have also been tried (Table 6). Free chlorine is most frequently used, but is known to rapidly degrade RO membranes in addition to producing the most disinfection by-products. Moreover, sometimes pre-chlorination or pre-ozonation can lead to enhanced bio-growth on RO membranes; they increase the AOC content of influent dissolved organic carbon (DOC) and, after it is quenched (typically, using sodium bisulfite), the water contains higher biogrowth potential and nothing to inhibit it<sup>79</sup>. Ozonation of bromide-rich saline waters can produce bromate, which is classified as a carcinogen by USEPA and WHO, and which, may not be completely rejected by RO membranes. UV treatment is gaining in popularity since it does not produce disinfection byproducts and quenches chlorine without adding

sodium bisulfite. However, it may not be effective where significant DOC or AOC exists in RO feed water because it only provides up front disinfection, but no residual bio-growth inhibition throughout the RO membrane system and it may break down some recalcitrant DOC into AOC. At a seawater RO demonstration plant, including chlorination, microfiltration and dechlorination pre-treatments alone, and followed by UV irradiation, UV pretreatment added no additional benefit<sup>80</sup>.

The use of chloramines can be an effective means to control RO membrane biofouling in wastewater reclamation plants<sup>81</sup>; although, some reports suggest chloramines are not effective for biofouling control<sup>82</sup>. Variances may come from different qualities of tertiary wastewater being fed into the RO membranes. Moreover, not all RO membrane manufacturers offer warranty coverage on their membranes when continuous chloramine dosing is part of the RO plant operational strategy. Combining membrane filtration and chloramination as pretreatment can be more effective at fouling control because it reduces influent colloidal matter while also inhibiting bio-growth. But concerns over membrane degradation in high chloride-containing waters (e.g., seawater) persist because the elevated oxidation potential can create trace amounts of chlorine from chloride ions.

Intermittent chlorine injection (ICI) has been demonstrated to successfully reduce biofouling on cellulose triacetate (CTA) membranes in seawater containing heavy metals, but a systematic

**Table 6.** Summary of bio-growth inhibitors, mechanisms, advantages and disadvantages.

Inhibitor	Mechanism(s)	Advantage(s)	Disadvantage(s)
Chlorine	Oxidative inhibition	Prevents biofilm at low doses Familiar to operators Well proven Accepted practice	Chlorination byproducts Membrane degradation
Chloramines	Oxidative inhibition	Prevents biofilm at moderate doses Familiar to operators Well proven Accepted practice	Chloramination byproducts Membrane degradation
Chlorine dioxide	Oxidative inhibition	Well proven bio-growth inhibitor Prevents biofilm at very low doses (~1ppm) Does not directly degrade RO membranes	Chlorite/chlorate only known byproducts Sometimes carries sufficient free chlorine residual that it degrades RO membranes
ICI	Oxidative shock	Periodically retards bio-growth Reduced byproducts Reduced degradation	Does not prevent biofilm formation Lack of operator familiarity Not well-proven for polyamide RO membranes
DBNPA	Releases 2,2-dibromo-3-nitripropionamide Degrades cell membrane protein leads to lysis	Used widely in industrial systems Can be combined with chlorine Meets FDA requirements EPA registered	More expensive than chlorine Lack of operator familiarity Not well-proven in water treatment
NO donors	DNA damage Degradation of iron sulfur centers	Non-oxidative, so compatible with RO membranes Inhibits bio-growth at lab scale	No regulatory approval More expensive than chlorine Lack of operator familiarity Not well-proven
DCC	Releases HOCl and isocyanuric acid Maintains low free available chlorine (FAC)	Used widely in swimming pools, industrial cooling systems, & hospitals	No regulatory approval More expensive than chlorine Lack of operator familiarity Not well-proven
Phosphorous removal	Lack of essential nutrient	Can be completely effective by making phosphorous the limiting nutrient	May not work if phosphorous is not a limiting nutrient Eliminates some highly effective antiscalants

ICI intermittent chlorine injection, DBNPA 2,2-dibromo-3-nitripropionamide, NO nitric oxide, DCC dichloroisocyanurate.

study was required to identify the optimal combination of dose, duration and frequency for the plant-specific feed water quality, pretreatment sequence and RO membrane array<sup>83</sup>. A non-oxidative biocide, 2,2-dibromo-3-nitripropionamide (DBNPA), can also be used to minimize and/or eliminate problems due to biofouling accumulation and to ensure long-term performance of a RO system<sup>84</sup>. DBNPA is compatible with RO membrane materials and is highly rejected by RO membranes, and has already been demonstrated successfully in field studies on full-scale RO systems<sup>85</sup>. The major drawback of this biocide is its cost, which is very high relative to conventional water treatment disinfectants, but could be economical if used intermittently.

Most recently, nitric oxide (NO) donor compounds proved effective at removing both biofilm bacteria cells and EPS with MAHMA-NONOate [6-(2-Hydroxy-1-methyl-2-nitroso hydrazino)-N-methyl-1-hexanamine, NOC-9] being the optimal NO donor compound<sup>53</sup>. Nitric oxide is toxic to bacteria; the mechanism for this includes DNA damage and degradation of iron sulfur centers into iron ions and iron-nitrosyl compounds. However, many bacterial pathogens have evolved mechanisms for NO resistance suggesting the same could happen in a RO membrane plant<sup>86</sup>. In another study, biofilms grown on RO membranes were inactivated by dichloroisocyanurate (DCC) as well as by chlorine; flux and rejection by DCC-exposed membranes were stable, while rejection by chlorine-exposed membranes decreased from ~99 to 80%<sup>87</sup>. Vrouwenvelder and co-workers have shown that phosphorous removal can greatly reduce biofilm formation on RO membranes<sup>88</sup>.

### RO membrane cleaning and biofilm removal

Membrane cleaning chemicals and protocols are prescribed by membrane manufacturers and chemical vendors, which typically are not involved until an RO plant is already experiencing major operational disruption. So, each scenario tends to be addressed ad hoc. While there are generalizable approaches to cleaning, there are no known universally successful protocols for cleaning fouled RO membranes. An alkaline clean is often performed before or after an acid clean when targeting removal of both organic and inorganic foulants. Typical cleaning agents include acids (citric acid, HCl, HNO<sub>3</sub>, H<sub>2</sub>SO<sub>4</sub>), bases (NaOH, NH<sub>3</sub>OH), complexing agents like EDTA, surfactants like SDS, and their combination<sup>89–95</sup>. In the case of organic and biological fouling, it is typical to apply alkaline cleaning solutions containing various combinations of surfactants, chelating agents, enzymes and chaotropic agents<sup>27,40,96</sup>.

In one recent study at a wastewater RO plant, two stages of caustic and detergent cleaning (NaOH + SDS) followed by acid provided effective recovery of initial RO membrane flux and rejection. Sometimes chlorine and other biocides are also applied as part of a cleaning regimen or intermittently between cleaning intervals as in the ICI method described above<sup>83,97</sup>. *To achieve the highest cleaning efficiency, the cleaning solution(s) chemistry, sequence, flow velocity, temperature, duration and frequency must be studied and optimized for a given RO installation—as they vary by water quality, type of fouling materials, type of RO membrane, RO pretreatment processes and RO system operating conditions.* Moreover, cleaning regimens may need updating as feed water



**Fig. 11 Pictures of various fouling detectors employed at a seawater desalination plant.** Research conducted at the Long Beach Water Department's seawater RO/NF demonstration plant focusing on NF/RO membrane biofouling mechanisms, prevention, and monitoring. Tanuwidjaja<sup>107</sup> compared three different membrane fouling detectors to understand potential bias due to different monitoring device configurations. At left, four parallel trains of 3 sensors per train are depicted. At right, a single train of 3 fouling detectors including UCLA's high-pressure fouling detector, which enables flux, rejection and differential pressure to be monitored as well as a UCLA low-pressure fouling detector and a KIWA/Wetsus low-pressure fouling detector; both low-pressure fouling detectors monitor differential pressure only. Original image courtesy of Dian Tanuwidjaja. Copyright University of California, Los Angeles.

quality, pretreatment efficacy, and RO membranes change over the life of a plant.

### Biofouling monitoring strategies

As mentioned above, one key to mitigating biofouling in RO systems is choosing an adequate biofilm monitoring technique that (1) gives an early warning indication of the onset of biofouling and (2) confirms the effectiveness of biofouling control measures employed. A recent trend in membrane research involves the use of *ex situ*, side-stream fouling detectors applied as early warning sensors at full-scale and pilot plants. For example, Vrouwenvelder and co-workers developed an *ex situ* fouling detector they called a "membrane fouling simulator" (MFS) to monitor biological fouling in RO and NF filtration of surface and ground water<sup>36,41</sup>. The MFS provided (i) the same hydraulic behavior as spiral wound membrane modules, (ii) reproducible results, and (iii) effective early warning of biological fouling by monitoring tangential pressure drop through the system. Subsequently, Vrouwenvelder and co-workers used the MFS to elucidate new fundamental insights into membrane biofouling mechanisms, particularly focusing on "fouling as a spacer problem" and methods of inhibiting biofilm formation and removing biofilms once formed<sup>28,30–35,37–39,42</sup>. A limitation of the MFS device is that it was designed for low pressure (<50 psi) operation such that there is no water permeation through NF/RO membranes in most applications.

Over the past decade, Hoek and co-workers extended the range of working pressures for optical fouling detectors from microfiltration (<50 psi) up to seawater RO (<1200 psi)<sup>21–26,98–106</sup>. In the course of this work, they derived insights about attachment and removal of bacteria cells on polymeric membranes, particularly focusing on Stage 1 (in Fig. 6) of biofilm formation. More recently, Hoek and Vrouwenvelder joined forces to evaluate the use of low-pressure (LP) and high-pressure (HP) fouling detectors (FDs) at the Long Beach Water Department (LBWD) desalination demonstration plant (Fig. 11)<sup>80,107</sup>. Permeate flux, TDS rejection, and differential pressure drop data derived from

two LPFDs did not correspond well with the full-scale plant, whereas the HPFD mimicked the full-scale plant behavior well. Moreover, the HPFD was much more sensitive than the full-scale plant. Hence, the HPFD gave early warning detection of fouling and membrane degradation and proved useful in optimizing membrane cleaning protocols.

Other researchers have employed similar fouling detector devices in lab and full-scale studies. For example, Cohen and co-workers extended a laboratory-scale optical membrane module into a novel, *ex situ* scaling observation detector (EXSOD)<sup>108</sup>. Subsequently, they used their EXSOD system to conduct a number of studies on the feasibility, scaling limits and optimized scale inhibition methods for RO desalination of brackish agricultural waters<sup>109–113</sup>. A more recent study by Duranceau and co-workers successfully employed sacrificial 4" by 40" spiral wound elements as "canary modules" to optimize chemical pretreatment at a brackish groundwater RO plant<sup>113</sup>. *Membrane fouling detector technology is available for anyone to employ and these devices can be used not only for early warning of RO membrane biofouling, but also for other forms of fouling, mineral scaling, membrane damage and cleaning efficacy in any membrane process.* *Ex situ, side-stream monitoring of RO membrane performance is now a practical reality and should be considered best practice for use at RO membrane plants.*

### CONCLUSION

The lack of chlorine tolerance by commercially available RO membranes makes it very difficult to prevent bio-growth, and hence, biofouling and its deleterious effects persist in all types RO membrane plants. Influent water quality, pretreatments, RO membranes, plant operating conditions are among the key factors that must be understood, studied, and continuously monitored. From a water quality perspective, critical parameters include influent bacteria cell concentration and viability (e.g., VBNC) and, perhaps most importantly, both consistent and episodic (e.g., algae bloom driven) feed water nutrient concentration (AOC, N, P).

Some combination of chlorination, media or membrane filtration, and dechlorination, in many cases, followed by acid and/or antiscalant addition appears the most common pre-treatment sequence. It is important to dechlorinate ahead of acid and antiscalant addition because organic biocides and polymeric compounds in such chemicals can be degraded by free chlorine and produce AOC. For low-pressure brackish and wastewater RO applications, combined chlorine is emerging as the best practice for minimizing biofouling, but it remains problematic and not viable for seawater RO plants. In some industrial applications non-oxidizing biocides are being applied, but most of these chemicals remain either too expensive or too toxic for use in large scale water treatment applications. Among a number of unique aspects of RO membrane biofouling, convective delivery of nutrients into the biofilm combined with flux hot spots and stagnant mass transfer zones exacerbate biofouling. Assuming biofouling is a substrate-limited growth problem, biofilms will form first in lead elements where both flux and influent nutrient concentration are the highest. As biofouling commences, lead elements lose productivity, but water flux shifts to down-stream elements with very little need to increase feed pressure. This makes it challenging to detect biofouling using plant-level performance indicators until the technology improves. Sufficient progress has been made in the development and deployment of ex situ, side-stream fouling detectors that it should be considered best practice to employ some form of fouling detection at all RO installations. Future work should focus on standardizing and commoditizing such fouling detection tools. Also, there remains a need for chlorine tolerant RO membranes, particularly in seawater RO. Certainly, chlorine tolerant polymers exist, but the historical challenge has been combining chlorine tolerance with flux and rejection on par with state-of-the-art polyamide composite RO membranes.

## DATA AVAILABILITY

The data sets generated during and/or analyzed during the current study are available from the corresponding author on reasonable request.

Received: 1 February 2021; Accepted: 4 August 2022;

Published online: 15 September 2022

## REFERENCES

- Bixler, G. D. Biofouling: lessons from nature. *Philos. Trans. R. Soc. a-Math. Phys.* **370**, 2381–2417 (2012).
- Mattilasandholm, T. Biofilm formation in the industry - a review. *Food Rev. Int.* **8**, 573–603 (1992).
- Meyer, B. Approaches to prevention, removal and killing of biofilms. *Int. Biodegrad. Biodegrad.* **51**, 249–253 (2003).
- Al-Juboori, R. A. Biofouling in RO system: mechanisms, monitoring and controlling. *Desalination* **302**, 1–23 (2012).
- Flemming, H. C. Biofouling - the Achilles heel of membrane processes. *Desalination* **113**, 215–225 (1997).
- Flemming, H. C. Reverse osmosis membrane biofouling. *Exp. Therm. Fluid Sci.* **14**, 382–391 (1997).
- Matin, A. Biofouling in reverse osmosis membranes for seawater desalination. *Desalination* **281**, 1–16 (2011).
- Ridgway, H. et al. Biofouling of membranes: membrane preparation, characterization, and analysis of bacterial adhesion. *Biofilms* **310**, 463–494 (1999).
- Hasan, J., Crawford, R. J. & Ivanova, E. P. Antibacterial surfaces: the quest for a new generation of biomaterials. *Trends Biotechnol.* **31**, 295–304 (2013).
- Herzberg, M. Osmotic effects of biofouling in reverse osmosis (RO) processes. *Desalination Water Treat.* **15**, 287–291 (2010).
- Sweity, A., Oren, Y., Ronen, Z. & Herzberg, M. The influence of antiscalants on biofouling of RO membranes in seawater desalination. *Water Res.* **47**, 3389–3398 (2013).
- Gutman, J. Interactions between biofilms and NF/RO flux and their implications for. *J. Membr. Sci.* **421**, 1–7 (2012).
- Tanuwidjaja, D. et al. Comparison of membrane fouling and cleaning in one-pass reverse osmosis and two-pass nanofiltration approaches to seawater desalination. *Desalination Water Treatment* **193**, 235–250 (2020).
- Zhang, M. et al. Composition and variability of biofouling organisms in seawater reverse osmosis desalination plants. *Appl. Environ. Microbiol.* **77**, 4390–4398 (2011).
- Edalat, A., Jawor, A., Tanuwidjaja, D., Bhattacharjee, S. & Hoek, E. M. V. *Water Planet Engineering Final Report: Santa Monica Ground Water RO Plant.* (2012).
- Hoek, E. M. V., Allred, J., Knoell, T. & Jeong, B.-H. Modeling the effects of fouling on full-scale reverse osmosis processes. *J. Membr. Sci.* **314**, 33–49 (2008).
- Gu, H. & Plumlee, M. Personal Communication. (2020).
- Jawor, A., Hoek, E. M. V. & Edalat, A. *STEEL INDUSTRY Part 1-Optimization of Pretreatment and Reverse Osmosis Desalination of Steel Plant Inorganic Wastewater Effluent.* [www.copyright.com](http://www.copyright.com) (2014).
- Jawor, A., Hoek, E. M. V., Edalat, A. & Kim, Y. O. *STEEL INDUSTRY Part 2: Analysis of Membranes Used To Treat Steel Plant Effluent.* [www.copyright.com](http://www.copyright.com) (2014).
- Whittaker, C., Ridgway, H. & Olson, B. H. Evaluation of cleaning strategies for removal of biofilms from reverse-osmosis membranes. *Appl. Environ. Microbiol.* **48**, 395–403 (1984).
- Kang, S., Hoek, E. M. V., Choi, H. & Shin, H. Effect of membrane surface properties during the fast evaluation of cell attachment. *Sep. Sci. Technol.* **41**, 1475–1487 (2006).
- Kang, S.-T., Subramani, A., Hoek, E. M. V., Deshusses, M. A. & Matsumoto, M. R. Direct observation of biofouling in cross-flow microfiltration: mechanisms of deposition and release. *J. Membr. Sci.* **244**, 151–165 (2004).
- Wang, S., Guillen, G. & Hoek, E. M. V. Direct observation of microbial adhesion to membranes. *Environ. Sci. Technol.* **39**, 6461–6469 (2005).
- Subramani, A. & Hoek, E. M. V. Direct observation of initial microbial deposition onto reverse osmosis and nanofiltration membranes. *J. Membr. Sci.* **319**, 111–125 (2008).
- Subramani, A., Huang, X. & Hoek, E. M. V. Direct observation of bacterial deposition onto clean and organic-fouled polyamide membranes. *J. Colloid Interface Sci.* **336**, 13–20 (2009).
- Huang, X., Guillen, G. R. & Hoek, E. M. V. A new high-pressure optical membrane module for direct observation of seawater RO membrane fouling and cleaning. *J. Membr. Sci.* **364**, 149–156 (2010).
- Subramani, A. & Hoek, E. M. V. Biofilm formation, cleaning, re-formation on polyamide composite membranes. *Desalination* **257**, 73–79 (2010).
- Vrouwenvelder, J. S. et al. Quantitative biofouling diagnosis in full scale nanofiltration and reverse osmosis installations. *Water Res.* **42**, 4856–4868 (2008).
- Vrouwenvelder, J. S. et al. The membrane fouling simulator: a suitable tool for prediction and characterisation of membrane fouling. *Water Sci. Technol.* **55**, 197–205 (2007).
- Creber, S. A. et al. Magnetic resonance imaging and 3D simulation studies of biofilm accumulation and cleaning on reverse osmosis membranes. *Food Bioprod. Process.* **88**, 401–408 (2010).
- Cornelissen, E. R. et al. Air/water cleaning for biofouling control in spiral wound membrane elements. *Desalination* **204**, 145–147 (2007).
- Cornelissen, E. R. et al. Periodic air/water cleaning for control of biofouling in spiral wound membrane elements. *J. Membr. Sci.* **287**, 94–101 (2007).
- von der Schulenburg, D. A. G., Vrouwenvelder, J. S., Creber, S. A., van Loosdrecht, M. C. M. & Johns, M. L. Nuclear magnetic resonance microscopy studies of membrane biofouling. *J. Membr. Sci.* **323**, 37–44 (2008).
- Vrouwenvelder, J. S., Hinrichs, C., van der Meer, W. G. J., van Loosdrecht, M. C. M. & Kruijthof, J. C. Pressure drop increase by biofilm accumulation in spiral wound RO and NF membrane systems: role of substrate concentration, flow velocity, substrate load and flow direction. *Biofouling* **25**, 543–555 (2009).
- Vrouwenvelder, J. S. et al. Phosphate limitation to control biofouling. *Water Res.* **44**, 3454–3466 (2010).
- Vrouwenvelder, J. S., van Paassen, J. A. M., Wessels, L. P., van Dama, A. F. & Bakker, S. M. The membrane fouling simulator: a practical tool for fouling prediction and control. *J. Membr. Sci.* **281**, 316–324 (2006).
- Vrouwenvelder, J. S., Kappelhof, J., Heijman, S. G. J., Schippers, J. C. & van der Kooij, D. Tools for fouling diagnosis of NF and RO membranes and assessment of the fouling potential of feed water. *Desalination* **157**, 361–365 (2003).
- Vrouwenvelder, J. S., van Paassen, J. A. M., Kruijthof, J. C. & van Loosdrecht, M. C. M. Sensitive pressure drop measurements of individual lead membrane elements for accurate early biofouling detection. *J. Membr. Sci.* **338**, 92–99 (2009).
- Prest, E. I., Staal, M., Kuhl, M., van Loosdrecht, M. C. M. & Vrouwenvelder, J. S. Quantitative measurement and visualization of biofilm O<sub>2</sub> consumption rates in membrane filtration systems. *J. Membr. Sci.* **392**, 66–75 (2012).
- Creber, S. A., Vrouwenvelder, J. S., van Loosdrecht, M. C. M. & Johns, M. L. Chemical cleaning of biofouling in reverse osmosis membranes evaluated using magnetic resonance imaging. *J. Membr. Sci.* **362**, 202–210 (2010).

41. Vrouwenvelder, J. S., Bakker, S. M., Wessels, L. P. & van Paassen, J. A. M. The membrane fouling simulator as a new tool for biofouling control of spiral-wound membranes. *Desalination* **204**, 170–174 (2007).
42. Radu, A. I., Vrouwenvelder, J. S., van Loosdrecht, M. C. M. & Picioreanu, C. Effect of flow velocity, substrate concentration and hydraulic cleaning on biofouling of reverse osmosis feed channels. *Chem. Eng. J.* **188**, 30–39 (2012).
43. Vrouwenvelder, J. S., Manolarakis, S. A., Veenendaal, H. R. & van der Kooij, D. Biofouling potential of chemicals used for scale control in RO and NF membranes. *Desalination* **132**, 1–10 (2000).
44. Vrouwenvelder, J. S., Kruithof, J. C. & van Loosdrecht, M. C. M. Integrated approach for biofouling control. *Water Sci. Technol.* **62**, 2477–2490 (2010).
45. Vrouwenvelder, J. S., van Loosdrecht, M. C. M. & Kruithof, J. C. A novel scenario for biofouling control of spiral wound membrane systems. *Water Res.* **45**, 3890–3898 (2011).
46. van der Kooij, D., Vrouwenvelder, J. S. & Veenendaal, H. R. Elucidation and control of biofilm formation processes in water treatment and distribution using the unified biofilm approach. *Water Sci. Technol.* **47**, 83–90 (2003).
47. Vrouwenvelder, J. S. & van der Kooij, D. Diagnosis, prediction and prevention of biofouling of NF and RO membranes. *Desalination* **139**, 65–71 (2001).
48. Vrouwenvelder, J. S. & van der Kooij, D. Diagnosis of fouling problems of NF and RO membrane installations by a quick scan. *Desalination* **153**, 121–124 (2003).
49. Vrouwenvelder, H. S. Biofouling of membranes for drinking water production. *Desalination* **118**, 157–166 (1998).
50. Chong, T. H., Wong, F. S. & Fane, A. G. The effect of imposed flux on biofouling in reverse osmosis: role of concentration polarisation and biofilm enhanced osmotic pressure phenomena. *J. Membr. Sci.* **325**, 840–850 (2008).
51. Sim, S. T. V., Suwarno, S. R., Chong, T. H., Krantz, W. B. & Fane, A. G. Monitoring membrane biofouling via ultrasonic time-domain reflectometry enhanced by silica dosing. *J. Membr. Sci.* **428**, 24–37 (2013).
52. Leslie, G. L., Schneider, R. P., Fane, A. G., Marshall, K. C. & Fell, C. J. D. Fouling of a microfiltration membrane by 2 Gram-negative bacteria. *Colloids Surf. a-Physicochem. Eng. Asp.* **73**, 165–178 (1993).
53. Barnes, R. J. et al. Optimal dosing regimen of nitric oxide donor compounds for the reduction of *Pseudomonas aeruginosa* biofilm and isolates from wastewater membranes. *Biofouling* **29**, 203–212 (2013).
54. Chen, X. et al. Dynamics of biofilm formation under different nutrient levels and the effect on biofouling of a reverse osmosis membrane system. *Biofouling* **29**, 319–330 (2013).
55. Suwarno, S. R. et al. The impact of flux and spacers on biofilm development on reverse osmosis membranes. *J. Membr. Sci.* **405**, 219–232 (2012).
56. Bradford, S. M., Palmer, C. J. & Olson, B. H. Assimilable organic-carbon concentrations in Southern California surface and groundwater. *Water Res.* **28**, 427–435 (1994).
57. Hong, S. K., Escobar, I. C., Hershey-Pyle, J., Hobbs, C. & Cho, J. W. Biostability characterization in a full-scale hybrid NF/RO treatment system. *J. Am. Water Works Assoc.* **97**, 101–110 (2005).
58. Jacobson, J. D. Phosphate limitation in reverse osmosis: An option to control biofouling? *Desalination Water Treat.* **5**, 198–206 (2009).
59. Saeed, M. O. Effect of dechlorination point location and residual chlorine on biofouling in a seawater reverse osmosis plant. *Desalination* **143**, 229–235 (2002).
60. Song, L., Hong, S., Hu, J. Y., Ong, S. L. & Ng, W. J. Simulations of full-scale reverse osmosis membrane process. *J. Environ. Eng.* **128**, 960–966 (2002).
61. Schock, G. & Miquel, A. Mass transfer and pressure loss in spiral wound modules. *Desalination* **64**, 339–352 (1987).
62. Lin, L. et al. Relative importance of geometrical and intrinsic water transport properties of active layers in the water permeability of polyamide thin-film composite membranes. *J. Membr. Sci.* **564**, 935–944 (2018).
63. Rittmann, B. E. & McCarty, P. L. *Environmental Biotechnology: Principles and Applications*. (McGraw-Hill Education, 2001).
64. Guillen, G. & Hoek, E. M. V. Modeling the impacts of feed spacer geometry on reverse osmosis and nanofiltration processes. *Chem. Eng. J.* **149**, 221–231 (2009).
65. Hou, J. et al. Bacterial density and biofilm structure determined by optical coherence tomography. *Sci. Rep.* **9**, 9794 (2019).
66. Baker, J. S. & Dudley, L. Y. Biofouling in membrane systems - a review. *Desalination* [https://doi.org/10.1016/S0011-9164\(98\)00091-5](https://doi.org/10.1016/S0011-9164(98)00091-5) (1998).
67. Kim, S. H., Kwak, S.-Y. & Suzuki, T. Positron annihilation spectroscopic evidence to demonstrate the flux-enhancement mechanism in morphology-controlled thin-film-composite (TFC) membrane. *Environ. Sci. Technol.* **39**, 1764–1770 (2005).
68. Ramon, G. Z. & Hoek, E. M. V. Transport through composite membranes, part 2: Impacts of roughness on permeability and fouling. *J. Membr. Sci.* **425**, 141–148 (2013).
69. Wong, M. C. Y., Lin, L., Coronell, O., Hoek, E. M. V. & Ramon, G. Z. Impact of liquid-filled voids within the active layer on transport through thin-film composite membranes. *J. Membr. Sci.* **500**, 124–135 (2016).
70. Ramon, G. Z., Wong, M. C. Y. & Hoek, E. M. V. Transport through composite membrane, part 1: is there an optimal support membrane? *J. Membr. Sci.* **415**, 298–305 (2012).
71. Huang, X., Bhattacharjee, S. & Hoek, E. M. V. Is surface roughness a “scapegoat” or a primary factor when defining particle-substrate interactions? *Langmuir* **26**, 2528–2537 (2010).
72. Hoek, E. M. V. & Agarwal, G. K. Extended DLVO interactions between spherical particles and rough surfaces. *J. Colloid Interface Sci.* **298**, 50–58 (2006).
73. Hoek, E. M. V., Bhattacharjee, S. & Elimelech, M. Effect of membrane surface roughness on colloid-membrane DLVO interactions. *Langmuir* **19**, 4836–4847 (2003).
74. Vrijenhoek, E. M., Hong, S. & Elimelech, M. Influence of membrane surface properties on initial rate of colloidal fouling of reverse osmosis and nanofiltration membranes. *J. Membr. Sci.* **188**, 115–128 (2001).
75. Subramani, A., Kim, S. & Hoek, E. M. V. Pressure, flow, and concentration profiles in open and spacer-filled membrane channels. *J. Membr. Sci.* **277**, 7–17 (2006).
76. Hoek, E. M. V. & Elimelech, M. Cake-enhanced concentration polarization: a new fouling mechanism for salt-rejecting membranes. *Environ. Sci. Technol.* **37**, 5581–5588 (2003).
77. Obaid, M. Practical solutions to problems experienced in open seawater RO plants. *Desalination* **120**, 137–142 (1998).
78. Palacin, L. G. Scheduling of the membrane module rotation in RO desalination plants. *Desalination Water Treat.* **51**, 352–359 (2013).
79. Kim, D. Biocide application for controlling biofouling of SWRO membranes - an overview. *Desalination* **238**, 43–52 (2009).
80. Tanuwidjaja, D. et al. Comparison of high pressure and low pressure fouling detectors at a full-scale reverse osmosis seawater desalination plant. *Desalination* Submitted (2021).
81. Bartels, C. R. Design considerations for wastewater treatment by reverse osmosis. *Water Sci. Technol.* **51**, 473–482 (2005).
82. Raffin, M., Germain, E. & Judd, S. Assessment of fouling of an RO process dedicated to indirect potable reuse. *Desalination Water Treat.* **40**, 302–308 (2012).
83. Fujiwara, N. Optimization of the intermittent chlorine injection (ICI) method for seawater desalination RO plants. *Desalination* **229**, 231–244 (2008).
84. Bertheas, U. Use of DBNPA to control biofouling in RO systems. *Desalination Water Treat.* **3**, 175–178 (2009).
85. Majamaa, K. Three steps to control biofouling in reverse osmosis systems. *Desalination Water Treat.* **42**, 107–116 (2012).
86. Janeway, C., Travers, P., Walport, M. & Shlomchik, M. *Immunobiology*. (Garland Science, 2004).
87. Yu, J., Baek, Y., Yoon, H. & Yoon, J. New disinfectant to control biofouling of polyamide reverse osmosis membrane. *J. Membr. Sci.* **427**, 30–36 (2013).
88. Bucs, S. S. et al. Review on strategies for biofouling mitigation in spiral wound membrane systems. *Desalination* **434**, 189–197 (2018).
89. Madaeni, S. S. & Samieirad, S. Chemical cleaning of reverse osmosis membrane fouled by wastewater. *Desalination* **257**, 80–86 (2010).
90. Madaeni, S. S. & Daneshvar, H. Chemical cleaning of reverse osmosis membranes fouled by dye bath effluent of a carpet manufacturing plant. *J. Indian Chem. Soc.* **81**, 584–589 (2004).
91. Madaeni, S. S. & Mansourpanah, Y. Chemical cleaning of reverse osmosis membranes fouled by whey. *Desalination* **161**, 13–24 (2004).
92. Madaeni, S. S., Sasanipour, A. & Zereshki, S. Chemical cleaning of reverse osmosis membrane fouled by apple juice. *J. Food Process Eng.* **34**, 1535–1557 (2011).
93. Madaeni, S. S., Sasanipour, A. & Zereshki, S. Chemical cleaning of reverse osmosis membrane fouled by sugar solution. *Asia-Pac. J. Chem. Eng.* **5**, 691–700 (2010).
94. Madaeni, S. S., Mohamamdi, T. & Moghadam, M. K. Chemical cleaning of reverse osmosis membranes. *Desalination* **134**, 77–82 (2001).
95. Sohrabi, M. R., Madaeni, S. S., Khosravi, M. & Ghaedi, A. M. Chemical cleaning of reverse osmosis and nanofiltration membranes fouled by licorice aqueous solutions. *Desalination* **267**, 93–100 (2011).
96. Kim, L. H., Jang, A., Yu, H. W., Kim, S. J. & Kim, I. S. Effect of chemical cleaning on membrane biofouling in seawater reverse osmosis processes. *Desalination Water Treat.* **33**, 289–294 (2011).
97. Boorsma, M. J. Monitoring and controlling biofouling in an integrated membrane system. *Desalination Water Treat.* **31**, 347–353 (2011).
98. Huang, X. & Hoek, E. M. V. Direct observation of bacterial adhesion to seawater RO membranes. in American Water Works Association Annual Conference and Exposition 2009, ACE 2009 (2009).



99. Hoek, E. M. V. & Subramani, A. Direct observation of microbial adhesion to polymeric membranes. *Abstr. Pap. Am. Chem. Soc.* **232**, 544 (2006).
100. Wang, S. & Hoek, E. M. V. Back-pulse optimization for fouling free microfiltration. *Abstr. Pap. Am. Chem. Soc.* **227**, U1040–U1040 (2004).
101. Huang, X. F. & Hoek, E. M. V. COLL 436-Direct microscopic observation of marine bacteria adhesion to seawater RO membranes. *Abstracts of Papers of the American Chemical Society* **235**, (2008).
102. Kang, S., Agarwal, G., Hoek, E. M. V. & Deshusses, M. A. Initial adhesion of microorganisms to polymeric membranes. in *Proc. - International Conference on MEMS, NANO and Smart Systems, ICMENS 2003* (2003). <https://doi.org/10.1109/ICMENS.2003.1222005>.
103. Tanuwidjaja, D., Hoek, E. M. V., Cheng, R. C. & Wattier, K. Development and application of ex situ fouling detectors and their use to analyze seawater desalination pretreatment processes. in *American Water Works Association Annual Conference and Exposition 2010, ACE 2010, Papers* (2010).
104. Tanuwidjaja, D., Hoek, E. M. V., Cheng, R. C. & Wattier, K. L. Simulating algal bloom in seawater and impacts on membranes by the use of fouling cells. in *Water Quality Technology Conference and Exposition 2010* (2010).
105. Tanuwidjaja, D., Marambio-Jones, C., Huang, S., Jiang, S. & Hoek, E. M. V. Evaluation of Seawater Desalination Pretreatment Processes using High Pressure and Low Pressure Membrane Fouling Detectors. *Desalination* Submitted (2013).
106. Hoek, E. M. V., Kang, S. & Deshusses, M. A. Observation, measurement and modeling of biocolloid deposition in crossflow membrane filtration. *Abstr. Pap. Am. Chem. Soc.* **225**, U806–U806 (2003).
107. Tanuwidjaja, D. R. Development and Application of Ex Situ Fouling Detectors to Elucidate Mechanisms of Seawater NF/RO Membrane Fouling and Degradation. Ph.D. Dissertation, Department of Civil & Environmental Engineering, University of California, Los Angeles (2010).
108. Uchymiak, M., Rahardianto, A., Lyster, E., Glater, J. & Cohen, Y. A novel RO ex situ scale observation detector (EXSOD) for mineral scale characterization and early detection. *J. Membr. Sci.* **291**, 86–95 (2007).
109. Bartman, A. R., Lyster, E., Rallo, R., Christofides, P. D. & Cohen, Y. Mineral scale monitoring for reverse osmosis desalination via real-time membrane surface image analysis. *Desalination* **273**, 64–71 (2011).
110. Lyster, E., Kim, M. M., Au, J. & Cohen, Y. A method for evaluating antiscalant retardation of crystal nucleation and growth on RO membranes. *J. Membr. Sci.* **364**, 122–131 (2010).
111. McCool, B. C. et al. Feasibility of reverse osmosis desalination of brackish agricultural drainage water in the San Joaquin Valley. *Desalination* **261**, 240–250 (2010).
112. Uchymiak, M. et al. Brackish water reverse osmosis (BWRO) operation in feed flow reversal mode using an ex situ scale observation detector (EXSOD). *J. Membr. Sci.* **341**, 60–66 (2009).
113. Tharamapalan, J., Boyd, C. C. & Duranceau, S. J. 3-Step approach towards evaluation and elimination of acid use in pre-treatment for a brackish water reverse osmosis process. *J. Environ. Manag.* **124**, 115–120 (2013).
114. Ridgway, H. Membrane materials: theory, chemistry, structure and the future. *Int Symp Membrane Biofouling. Science & Solutions* (2010).

## ACKNOWLEDGEMENTS

Funding for the production of this manuscript was provided by Water Planet Engineering as well as the UCLA Samueli Engineering School, the UCLA Department of Civil & Environmental Engineering and the UCLA Sustainable LA Grand Challenge. T.M.W. performed the biofouling modeling work as part of a classroom research project for course credit when he was enrolled in CEE258A as a M.S. student in the UCLA Department of Civil & Environmental Engineering.

## AUTHOR CONTRIBUTIONS

E.M.V.H. was responsible for acquisition of funding, conception and design of the work, the acquisition, analysis, and interpretation of data, and drafting and substantively revising the manuscript. T.M.W. performed the biofouling model coding and simulations, analysis and interpretation of data and drafted the original biofouling model study incorporated herein, and substantively revising the manuscript. A.E. was responsible for the conception and design, acquisition, analysis and interpretation of data and drafting the report on the biofouling case study in the Section “Brackish groundwater” while working at Water Planet Engineering.

## COMPETING INTERESTS

The authors declare no competing interests.

## ADDITIONAL INFORMATION

**Correspondence** and requests for materials should be addressed to Eric M. V. Hoek.

**Reprints and permission information** is available at <http://www.nature.com/reprints>

**Publisher's note** Springer Nature remains neutral with regard to jurisdictional claims in published maps and institutional affiliations.



**Open Access** This article is licensed under a Creative Commons Attribution 4.0 International License, which permits use, sharing, adaptation, distribution and reproduction in any medium or format, as long as you give appropriate credit to the original author(s) and the source, provide a link to the Creative Commons license, and indicate if changes were made. The images or other third party material in this article are included in the article's Creative Commons license, unless indicated otherwise in a credit line to the material. If material is not included in the article's Creative Commons license and your intended use is not permitted by statutory regulation or exceeds the permitted use, you will need to obtain permission directly from the copyright holder. To view a copy of this license, visit <http://creativecommons.org/licenses/by/4.0/>.

© The Author(s) 2022